Developing a tile drainage module for the Cold Regions Hydrological Model: Lessons from a farm in Southern Ontario, Canada

Mazda Kompanizare[*&#], Diogo Costa[+*], Merrin L. Macrae[&], John W. Pomeroy[*], Richard M. Petrone[&]

[*]**Centre for Hydrology, University of Saskatchewan, Canmore and Saskatoon, Canada**

[+] **Mediterranean Institute for Agriculture, Environment and Development, University of Évora, Portugal**

[&]**University of Waterloo, Waterloo, Canada**

[#]**Corresponding author: kompanizare.mazda@usask.ca**

Abstract

Systematic tile drainage is used extensively in poorly drained agricultural lands to remove excess water and improve crop growth; however, tiles can also transfer nutrients from farmlands to downstream surface water bodies, leading to water quality problems. Thus, there is a need to simulate the hydrological behaviour of tile drains to understand the impacts of climate or land management change on agricultural surface and subsurface runoff. The Cold Regions Hydrological Model (CRHM) is a physically based, modular modeling system developed for cold regions. Here, a tile drainage module is developed for CRHM. A multi-variable, multi-criteria model performance evaluation strategy was deployed to examine the ability of the module to capture tile discharge under both winter and summer conditions (NSE>0.29, RSR<0.84 and PBias <20 for tile flow and saturated storage simulations). Initial model simulations run at a 15-min

interval did not satisfactorily represent tile discharge; however, model simulations improved when the time step was lengthened to hourly but also with the explicit representation of capillary rise for moisture interactions between the rooting zone and groundwater, demonstrating the significance of capillary rise above the saturated storage layer in the hydrology of tile drains in loam soils. Novel aspects of this module include the sub-daily time step, which is shorter than most existing models, and the use of field capacity and its corresponding pressure head to provide estimates of drainable water and the thickness of the capillary fringe, rather than using detailed soil retention curves that may not always be available. An additional novel aspect is the demonstration that flows in some tile drain systems can be better represented and simulated when related to shallow saturated storage dynamics.

Keywords: tile drainage, cold regions, hydrological model, capillary fringe, drainable water, saturated storage fluctuations

1. Introduction

Harmful algal blooms and eutrophication in large freshwater lakes surrounded by agricultural lands are major environmental challenges in Canada and globally. The transport of nutrients, particularly phosphorus, in runoff from agricultural fields into surface water is an important contributor to the increased frequency of algal blooms being experienced in North America and elsewhere (Sharpley et al., 1995; Correll, 1998; Filippelli, 2002; Ruttenberg, 2005; Schindler, 2006; Quinton et al., 2010; Costa et al., 2022). Although nutrient transport from agricultural fields

2

45 can occur via both surface runoff and tile drainage (Radcliffe et al., 2015), recent increases in the

46 frequency and magnitude of algal blooms in Lake Erie in North America have been attributed to

47 tile drainage (King et al., 2015; Jarvie et al., 2017). Tile drain systems lower seasonally high-water

48 tables in poorly drained fields, reduce the retention time of soil water, lessening waterlogging in

49 fields and improving both crop growth and field trafficability for farmers (Cordeiro and Ranjan,

50 2012; Kokulan et al., 2019a). However, they are also important pathways for dissolved nutrients

51 and particulate material (Kladivko et al., 1999; Tomer et al., 2003). In Alberta, tile drains have

52 also been used to address salinity issues (Broughton and Jutras, 2013). It has been estimated that

53 14% of farmlands in Canada (ICID, 2018) and 45% of fields in Southern Ontario, Canada (ICID,

54 2018; Kokulan, 2019) are drained by tile systems. Given their importance in hydrological budgets

55 and biogeochemical transport, there is a need to understand the controlling mechanisms of water

56 and nutrient export from tile systems as an integral part of the broader, modified hydrological

57 system.

58   There are several models that can represent tile drainage, controlled tile drainage and

59 surface runoff in different soil types at the small basin scale, which typically calculate the amount

60 of gravitational drainage from the soil, such as HYPE (Lindstrom et al., 2010; Arheimer et al.,

61 2015), DRAINMOD (Skaggs, 1978, 1980a; Skaggs et al., 2012), MIKE SHE (Refsgaard and

62 Storm, 1995) and SWAT (Arnold et al., 1998; Koch et al., 2013; Du et al., 2005; Du et al., 2006;

63 Green et al., 2006; Kiesel et al., 2010). These models include conceptual components for many

64 key hydrological processes, and have been primarily designed and tested for temperate regions

65 (Costa et al., 2020a). In Canada and other cold regions, some unique hydrological processes such

66 as snowmelt, rain on snow, and runoff over and infiltration into frozen or partially-frozen soils

67 may also be important (Rahman et al., 2014; Cordeiro et al., 2017; Pomeroy et al., 1998, 2007;

68 Fang et al., 2010, 2013). Many hydrological processes, such as the sublimation of snow, energy

69 balance snowmelt, and infiltration into frozen soils, are strongly affected by temperature and the

70 phase changes of water, which make many existing models developed for warm regions less

71 appropriate for regions with cold seasons (Pomeroy et al., 2007, 2013, 2016; Fang et al., 2010,

72 2013). Even for temperate regions, the representation of cold season processes is often

73 underrepresented in models (Costa et al., 2020a).

74   Since the use of tile drainage is increasing in many cold regions (Kokulan et al., 2019a;

75 OMAFRA, 2023), it has become important to integrate such human-induced processes in the

76 specialized hydrological modelling tools that have been developed for these regions, such as the

77 Cold Regions Hydrological Modelling platform (CRHM, Pomeroy et al., 2007; 2013; 2022).

78 CRHM was initially developed in 1998 to assemble and explore the hydrological understanding

79 developed from a series of research basins spanning Canada and elsewhere into a flexible, modular,

80 object-oriented, multiphysics platform for simulating hydrological processes and basin response

81 in cold regions (Pomeroy et al., 2007; 2022). The modular CRHM platform allows for multiple

82 representations of forcing data interpolation and extrapolation, hydrological model spatial and

83 physical process structure and parameter values.

84   Many existing models typically operate at default daily or monthly time intervals, which

85 is inadequate for the prediction of many short-duration "flashy" hydraulic events observed in tiles

86 (Pluer et al., 2020; Vivekananthan, 2019; Vivekananthan et al., 2019; Lam et al., 2016a, 2016b;

87 Macrae et al., 2019). Indeed, the ability to simulate shorter time intervals (e.g., hourly) facilitates

88 the ability to capture both the rising and falling limbs of tile flow hydrographs, as well as the

89 magnitude of peak flows, both of which are important to tile drain chemistry and export

90 (Rozemeijer et al., 2016; Williams et al., 2015, 2016; Macrae et al., 2019).

91   The amount of water transported by tiles depends on soil moisture dynamics, hydraulic

92   gradients and the positioning of the saturated storage layer, which are in turn affected by many

93   factors, including soil type, surface topography and morphology, as well as the local climate and

94   the hydrological characteristics of the field (Frey et al. 2016; Klaiber et al., 2020; Coelho et al.,

95   2012; King et al., 2015). Thus, to provide reliable estimations of water loss from farmland via

96   surface runoff and tile flow, models must be able to predict soil moisture and saturated layer

97   storage (Brockley, 1976; Rozemeijer et al., 2016; Javani-Jouni et al., 2018). Early studies have

98   shown that in some soil types, including silty loam and clay loam soils, the drainable water is less

99   than expected based on the effective porosity (*e.g.*, Skaggs et al., 1978; Raats and Gardner, 1974).

100   Raats and Gardner (1974) have argued that the calculation of drainable porosity requires

101   knowledge of water table elevation and the distribution of soil moisture above the saturated storage

102   layer. Skaggs et al. (1978) added that the calculation of drainable porosity should consider "the

103   unsaturated zone drained to equilibrium with the water table". However, because the soil column

104   is often composed of different soil layers with varying physical characteristics, drainable porosity

105   varies with evapotranspiration rate, soil water dynamics and the depth of saturated water (Logsdon

106   et al., 2010; Moriasi et al., 2013). In a sandy loam soil, Lam et al. (2016a, 2016b) demonstrated

107   that tile drainage was not initiated until soil was at or above field capacity. Williams et al. (2019)

108   observed in the American Midwest that tile drainage was not initiated until the field storage

109   capacity had been exceeded. It has also been shown that despite the presence of tile drains, the soil

110   above the tile did not always drain all the gravitational water following a rainfall/snowmelt event

111   and the soil may remain at or above field capacity (Skaggs et al., 1978; Lam et al., 2016a). This

112   means that the soil drainable water content may be considerably smaller than the storage capacity.

113   This is related to matric potential within the vadose zone, which is driven by the soil characteristics

114   but can also be due to the development of a capillary fringe that reduces the rate of vertical

115   percolation through the unsaturated zone, reducing tile flow (Youngs, 2012). Despite this

116   evidence, some saturated flow models that simulate tile flow overlook the effect of capillary rise

117   and over-estimate the soil drainable water. Other models that represent unsaturated flow (i.e.,

118   HYDRUS 3D, Simunek et al., 2011) using Richard's Equation (Richards, 1931) capture the effect

119   of capillary rise and saturation-pressure variation within the soil profile and assess the soil

120   drainable water more accurately. Although the effect of capillary rise is considered in

121   DRAINMOD through the concept of drainable porosity (represented as a "water yield") (Skaggs,

122   1980b), and is calculated for layered soil profiles (Badr,1978), it requires detailed information

123   surrounding the soil water characteristic curve (Skaggs, 1980b). Although it is indeed optimal to

124   use soil-specific water characteristic curves, Twarakavi et al. (2009) found that it is possible to

125   employ average representative values from the soil water characteristic curve to represent soil

126   drainable water where soil-specific curves are not available, with some reduction in model

127   performance.

128   In this study, a new Tile Drainage Module (TDM) was developed and incorporated within

129   the physically based, modular Cold Regions Hydrological Modelling (CRHM) platform (Pomeroy

130   et al., 2022) to enable hydrological simulations in tile-drained farm fields in cold agricultural

131   regions. As a first iteration, the new module was developed for a field with sloping ground and

132   loam soil with imperfect drainage. Such landscapes are common in the Great Lakes Region (e.g.,

133   Michigan and Vermont, USA and Ontario, Canada) and tile drainage in such landscapes has not

134   been as widely studied as it has been in clay-dominated soil. In this module, considerations were

135   explicitly included for the effects of capillary rise and annual fluctuations in saturated storage on

136   drainable soil water storage. The use of field capacity and groundwater/soil saturated storage

137 (Twarakavi et al., 2009) to modulate soil drainable water across the soil profile, including the

138 capillary fringe region, is an innovative aspect of the model that has been demonstrated to

139 circumvent the need for water characteristic curves. The development of this physically based

140 module provides insight into hydrological processes in tile drainage from sloping landscapes with

141 imperfect drainage, which are increasingly being artificially drained (Cordeiro and Ranjan, 2012;

142 Kokulan et al., 2019a; OMAFRA, 2023).

143

144 **2.   Materials and Methods**

145 *2.1   Study area*

146 The study site is a ~10 ha farm field located near Londesborough, Ontario at UTM 17T 466689m

147 E, 4832203m N, shown as LON in Fig. 1a. Mean annual precipitation recorded in this region is

148 1247 mm (ECCC, 2020). Mean air temperature is 7.2 $^{\circ}$C, with annual maxima in July (25.9 $^{\circ}$C)

149 and minima in January (-10.2 $^{\circ}$C), (ECCC, 2020). Soil type has been identified as Perth clay loam

150 (Gr. Br. Luvisolic), with a slope between 0.2 and 3.5%. The field is systematically drained with a

151 tile depth of 0.9 m and a spacing of 14 m (laterals). The tile network collects infiltrated water from

152 about 75% of the field (~ 7.6 ha) but may also receive lateral groundwater flow from neighbouring

153 fields. Water yields from the tile drain laterals (10 cm diameter) are discharged via a common tile

154 outlet (main, 15 cm diameter) below ground. Surface runoff from the field is directed toward a

155 common outlet on the surface using plywood berms installed along the field edge (see van

156 Esbroeck et al., 2016). The tile and surface runoff outlets do not join into a common outlet and are

157 fully separated from one another, even during surface ponding events. The field is a corn-soy-

158 winter wheat rotation with cover drops and rotational conservation till (shallow vertical tillage

159 every three years). Additional details related to farming practices are provided in Plach et al.

7

160   (2019), soil characteristics are provided in Plach et al. (2018a) and Plach et al. (2018b) and

161   equipment and monitoring are provided in van Esbroeck et al., (2016). The outlets for both surface

162   and tile flow are located at the edge of the field and drain into an adjacent field (Fig. 1b). Water

163   tends to accumulate in a topographic low in the field, in front of the field outlet during snowmelt

164   or high-intensity rainfall events, presumably due to either surface runoff or return flow (see ponded

165   area, Fig. 1b). However, surface water or elevated soil moisture conditions are not observed in this

166   topographic low during smaller events or dry periods of the year, suggesting that this saturated

167   ponding is not in a perennial groundwater discharge zone. Although surface ponding is observed

168   in the topographic depression within the field, water discharges freely at the opposite end of the

169   culvert, facilitating the measurement of flow.

170
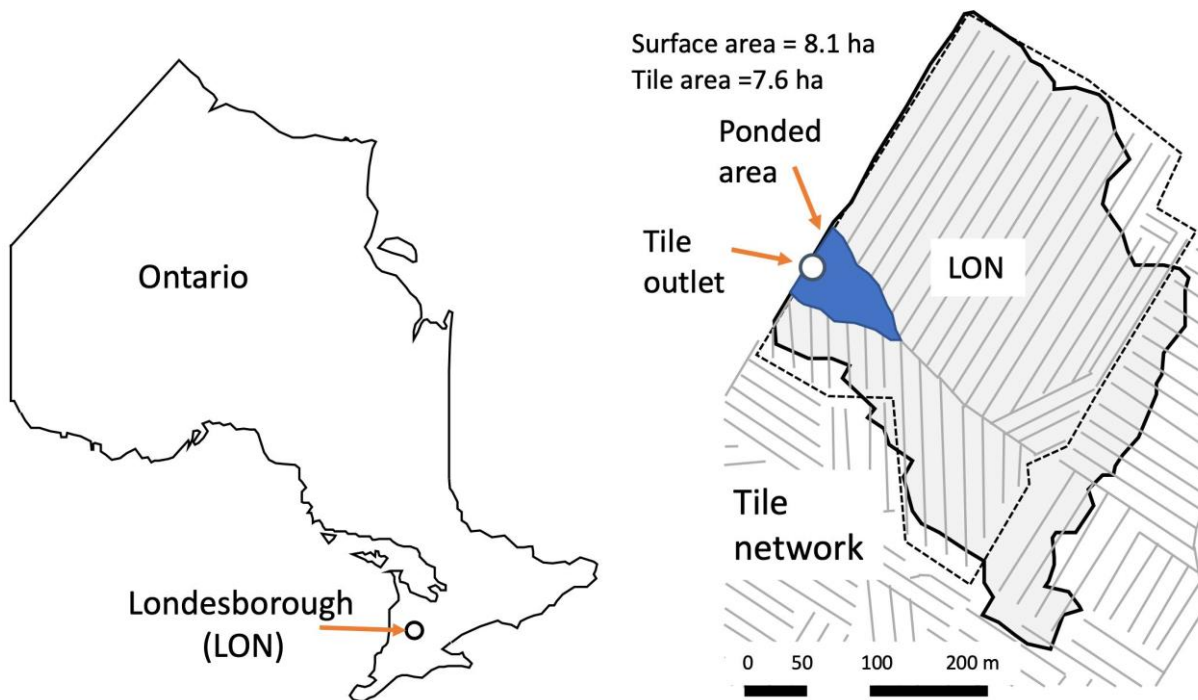
172   a)   b)

173   b)   Figure 1. (a) Location of the study area in South of Ontario and the (b) Londesborough (LON) farm with its tile network.

174

175

2.2   CRHM: The modelling platform

CRHM is a modular hydrological process modelling platform that allows users to select relevant process modules and apply them as needed to their study. For example, the CRHM platform includes options for empirical and physically based calculations of precipitation phase, snow redistribution by wind, snow interception, sublimation, sub-canopy radiation, snowmelt, infiltration into frozen and unfrozen soils, hillslope water movement, actual evapotranspiration, wetland fill and spill, soil water movement, groundwater flow and streamflow (Pomeroy et al., 2007; 2022). Where appropriate, it is able to calculate runoff from rainfall and snowmelt as generated by infiltration excess and/or saturated overland flow, flow over partially frozen soils, detention flow, shallow subsurface flow, preferential flow through macropores and groundwater flow (Pomeroy et al., 2007; 2022). Modules of a CRHM model can be customized to basin setup, such as delineating and discretizing the basin, conditioning observations for extrapolation and interpolation in the basin, or are process-support algorithms such as for estimating longwave radiation, complex terrain wind flow, or albedo dynamics, but most modules address hydrological processes such as evapotranspiration, infiltration, snowmelt, and streamflow discharge. CRHM discretizes basins into hydrological response units (HRU) for mass and energy balance calculations, each with unique process representations, parameters, and position along flow pathways in the basin. HRU are connected by blowing snow, surface, subsurface and groundwater flow and together generate streamflow which is routed to the basin outlet. The size of HRUs is flexible and can be as small as the size of a single tile pipe (e.g., 1 m) times the pipe spacing (which was 14 m in our case study region), and as large as entire tile networks within a given farm or study area. CRHM does not require a stream within a modelled basin. The feature allows CRHM

9

198   to model the hydrology of cold regions dominated by storage and episodic runoff, such as

199   agricultural fields.

200   Although CRHM has the capability to represent many hydrological and thermodynamic

201   processes, not all processes need/must be represented in all situations. The modular design of the

202   CRHM platform enables the user to activate or inactivate specific processes to optimize the model

203   for a particular situation. This is a modelling approach that enables testing different modelling

204   hypotheses and has been pioneered by CRHM and other models, which has inspired a range of

205   hydrological (e.g., SUMMA, Clark et al., 2015a, 2015b), hydrodynamic (e.g., mizuRoute,

206   Mizukami et al., 2016) and biogeochemical (e.g., OpenWQ, Costa et al., 2023) modelling tools.

207   For example, in the current study, blowing snow was not employed in CRHM as it does not appear

208   to be significant at the study site (periodic snow surveys showed relatively uniform snow cover).

209   Similarly, preferential flow into tile drains was not included in the current simulation. Although it

210   can be a key process in some clay loam soils, previous studies at the study site have shown that it

211   is not the case here, which is a combination of clay-loam and silt-loam soils (Pluer et al., 2020;

212   Macrae et al., 2019). Hydrograph analysis (Macrae et al., 2019) and conservative tracer (electrical

213   conductivity and major ions, as well as temperature) over multiple years (Pluer et al., 2020) showed

214   that preferential flow was minimal at this site as well as other similar sites. Freeze-thaw of soil can

215   occur in the study region, leading to partially frozen soils. However, the extent of freezing varies

216   with snowpack development, winter temperatures and radiation. Data collected over an 8-year

217   period at this site found soil freezing was restricted to brief periods and such freezing never

218   extended below 10 cm depth (Macrae, unpublished data) which is insufficient for soils to behave

219   as frozen ground for infiltration calculations. Consequently, freeze-thaw processes were not

220   deployed in the CRHM model of this site.

221

2.3   Observations and input data for the model

Tile flow, water table elevation (saturated storage elevation head) and surface flow were measured at the site between Oct. 2011 and Sept. 2018 at 15-minute intervals. It was not possible to install more than one measuring station for water table elevation and soil moisture at the site due to farming activity; consequently, water table elevation head and soil moisture were measured at the approximate midpoint of the field at the edge-of-field. Both tile flow rates and surface runoff were determined using simultaneous measurements of flow velocity and water depths in each of the pipes at the edge-of-field using Hach Flo-tote sensors and an FL900 data logger (Onset Ltd.) (Table A1, Appendix A). Continuous measurements of velocity were included due to the potential for impeded drainage under very wet conditions or caused by the accumulation of snow and ice around the surface culvert in winter. An additional barometrically-corrected pressure transducer (U20, Onset Ltd.) (Table A1) was also used for periods when the flow sensors did not function using a rating curve developed from the depth-velocity sensors; however, it should be noted that these were for brief periods and the depth-velocity sensor functioned for the majority of the study. The water table elevation was measured using a barometric pressure-corrected pressure transducer (U20, Onset Ltd.).

Air temperature, wind speed, air relative humidity, incoming solar irradiance and rainfall were also measured at the site at 15-minute intervals and were implemented in the model. Variable names and their symbols in CRHM are listed in Appendix B. The air temperature, wind speed and incoming solar radiance measurements were collected 1 m above ground using a Temperature Smart Sensor S-THB-M002, Wind Smart Sensor Set S-WSET-M002 and a Solar Radiation Sensor (Table A1). Rainfall and relative humidity were measured via a tipping bucket rain gauge (Table

11

244   A1) and an RH Smart Sensor (Table A1). These observations were continuously recorded

245   throughout the study period, except for brief periods of instrument failure and maintenance, when

246   data from nearby stations (Table T1, Supplementary Material) was substituted using the double

247   mass analysis method (Searcy and Hardison, 1960).

248   Although rainfall was recorded continuously at the field site, snowfall data was not.

249   Snowfall data was obtained from nearby stations (Wroxeter-Davis and Wroxeter, Environment

250   Canada, 2020), located 31.7 km from the field site. Periodic snow surveys done at the site

251   throughout the study period found that data from the nearby stations was a close approximation of

252   snow at the field site (Plach et al., 2019). Hourly snowfall observations from Wroxeter-Geonor

253   were used for the period between 2015 and 2018, whereas daily data from the Wroxeter-Geonor

254   were used for the 2011 to 2014 period, reconstructed to hourly snowfall time series based on the

255   method presented by Waichler and Wigmosta (2003).

256

257   *2.4   Development of the new tile module*

258   A Tile Drainage Module (TDM) was developed within CRHM (Figures 2, 3) with the goal of

259   adding the ability to simulate tile flow and the resulting saturated storage at an hourly time step.

260   CRHM was forced with hourly precipitation, air temperature, solar radiation, wind speed and

261   relative humidity to calculate hydrological states and fluxes in HRUs and the basin. The model

262   requires parameterizations that specify the hydraulic and hydrological properties of the soil,

263   including its thickness, saturated hydraulic conductivity (K), and surface cover. CRHM calculates

264   water storage and fluxes between HRUs, as well as vertical fluxes amongst different hydrological

265   compartments (within each HRU) that include snow, depressional storage, different soil layers,

266   and groundwater.

267   Using the simulation of soil moisture (including both saturated and unsaturated soil

268   moisture) performed by the original CRHM "*Soil*" module, TDM calculates the dynamic tile flow

269   rate that, in turn, feeds back to soil moisture at each time step. The presence of a capillary fringe

270   (sometimes referred to as the tension-saturated zone within the soil profile) and its effects are

271   considered by limiting the amount of drainable soil water. TDM uses site-specific information

272   regarding the tile network, such as tile depth, diameter and spacing. Information regarding site-

273   specific details regarding tile depth, diameter and spacing may be obtained directly from

274   landowners or can be estimated based on standard design and installation guidelines for the region.

275   This information was used to set up the model together with parameterization to translate the

276   hydrological effects of the soil capillary fringe (CF), if present, through two variables, CF

277   thickness and CF drainable water (discussed in Section 2.5, Figures 2, 3). These two variables are

278   used to limit the fraction of the soil moisture that can freely drain to the tiles.

279

280   *2.4.1   Soil moisture and saturated storage*

281   The TDM uses the water quality soil module or soil module (*WQ_soil* or *Soil*), which divides the

282   soil column into three layers: a recharge layer where evapotranspiration and root uptake generally

283   take place, a deeper layer that connects to the groundwater system and a deeper groundwater layer

284   that is always saturated. CRHM's state variable for soil moisture in the upper two layers is soil

285   water storage volume (Fig. 2), the model results were converted into water table elevation above

286   the semi-permeable layer (Table B1, Appendix B; Fig. 2b) for comparison with water table

287   observations, by dividing volumetric soil moisture content (Table B1) by soil porosity (Table B1)

288   for the cases with no capillary fringe above the water table. Additional steps were taken for periods

289   when a capillary fringe developed (discussed below).

290

2.4.2   Capillary fringe and drainable water

Soil moisture in the capillary fringe is equal to the average volumetric water content at capillary fringe (θ_C) which is usually greater than the field capacity (θ_{fc}) (Bleam, 2017, Sect. 2.4). Therefore, while the positioning of the capillary fringe responds dynamically to the matric potential, the saturation profile within the capillary fringe remains constant, as well as its thickness because it only depends on the pressure head (capillary forces) that are related to the grain size distribution and field capacity (h_{fc}) as introduced by Twarakavi et al. (2009). Therefore, the drainable water in the capillary fringe becomes the difference between saturation (θ_s), computed dynamically in CRHM, and θ_C, which corresponds to the water held by capillary forces at the capillary fringe moisture content (Fig. 2). Accordingly, Fig. 2 shows the schematic soil characteristic curve for the three water level conditions contemplated in the model.

1. *Condition 1* is when the water table is at the surface and the soil is completely saturated (matric potential = 0);

2. *Condition 2* is when the water table drops but the upper boundary of the capillary fringe is at the soil surface; and

3. *Condition 3* is when the water table drops further, and the upper boundary of the capillary fringe drops beneath the surface.

In essence, the soil is completely saturated (θ_s) in *Condition 1*. Between *Conditions 1* and *2*, the capillary fringe occupies the entire soil column above the water level; thus, it can only release the volume of water corresponding to θ_s-θ_C or φ_c (dimensionless). Between *Conditions 2* and *3*, two layers with distinct hydraulic characteristics develop: (1) the top one at θ_{fc} that releases water up

14

312   to θ_C-θ_{fc}, and (2) the lower one that corresponds to the capillary fringe and can release up to the

313   volume of water corresponding to θ_s-θ_C or φ_c.
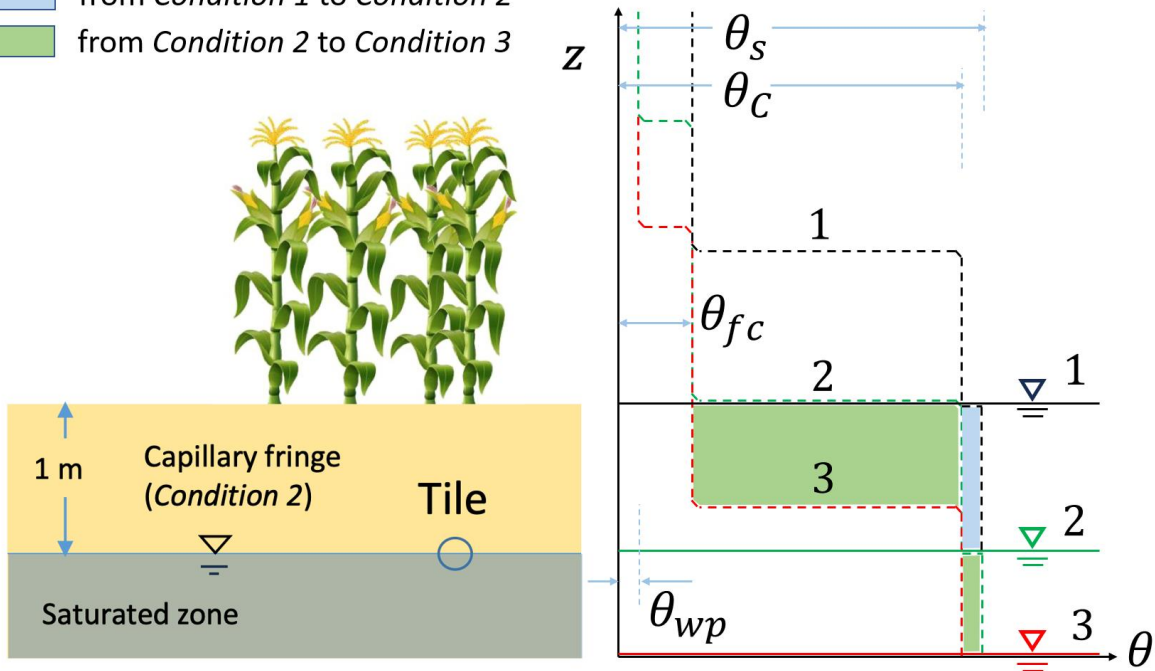
314

315   Figure 2. Schematic representation of the capillary fringe above the water table assuming a 1-m thickness (for demonstration

316   purposes). The soil characteristic curves are shown for the three water level conditions considered: water level at the (1) surface,

317   (2) intermediate depth, and (3) deeper depth. Two transitional drops can be seen in the characteristic curves, one from saturation

318   (θ_s) to capillary fringe water content (θ_C) (between *Conditions 1* and *2*) and one from θ_C to field capacity (θ_{fc}) (between *Conditions*

319   *2* and *3*). The coloured areas (green and blue) of the right panel correspond to the amount of water that can be released between

320   *Conditions 1* and *2* (blue) and between *Conditions 2* and *3* (green).

321

322

323   *2.4.3   Tile flow calculation*

324   A modified version of the Hooghoudt equation was used to calculate tile flow in the TDM

325   (Smedema et al., 2004). This presumes no surface ponding, an assumption that generally holds at

326 the study site (Eq. 1), where water ponds only during very wet periods and on a small portion of

327 the study site (see Fig. 1b). Hooghoudt's equation (Hooghoudt, 1940) is a steady state, physically

328 based equation for saturated flow toward the tile drain. Flow estimates are provided based on the

329 hydraulic conductivity of the soil and water table elevation above the tile pipe. It allows different

330 saturated hydraulic conductivities for the layers above (AL) and below (BL) the tile (Fig. S1). At

331 the study site, soil surveys have reported almost the same soil type (Loam) down to the depth of

332 90 cm (*e.g.,* Van Esbroeck et al., 2016; Plach et al., 2018b), which was parameterized in the model

333 set up as,

334

335 $$q = \frac{8 \times K_2 \times d \times h}{L^2} + \frac{4 \times K_1 \times h^2}{L^2} \,,$$ (1)

336

337 where K_1 and K_2 are respectively the saturated hydraulic conductivity in the upper and lower layers

338 in mm h^{-1}; L is the tile spacing in mm; h is the water table elevation above the tile in mm, d is the

339 lower layer thickness in mm (Fig. S1), and q is the predicted tile flow in mm h^{-1}. The only variable

340 that is dynamically updated by CRHM is h. Equation (1) was used to estimate tile flow rates in

341 TDM, using saturated storage to estimate h.

342

343 *2.4.4   Calculation of the effect of tile flow on soil moisture and water levels*

344 The simulated tile flows (see Sect. 2.3.3) were subtracted from the soil moisture. To calculate

345 saturated storage (water table or groundwater elevation head level) from soil moisture calculated

346 by the model, a threshold soil moisture content (sm_t) is defined, which consists of drainable water

347 in the soil (φ_c) when the upper boundary of the capillary fringe is at the surface (*Condition 2*, Fig.

348 2) and was calculated as:

349

$$sm_t = sm_{max} - (C_t \times \varphi_c) \quad ,$$
(2)

351

352 where sm_{max} is the maximum soil moisture and C_t is the capillary fringe thickness in mm.

353 However, since the hydrological conditions of the soil are markedly different between the two

354 transitional situations described in Sect. 2.3.2 and Fig. 2 (*Condition 1 to 2* and *Condition 2 to 3*),

355 a step function was deployed for determination of saturated storage :

356

357
$$SS = \begin{cases} \dfrac{sm_t - \left(C_t \times \left((\varphi_s - \varphi_c) + \theta_{fc}\right)\right)}{\varphi_s + \theta_{fc}} + \dfrac{sm - sm_t}{\varphi_c} & , if\ between\ Conditions\ 1\ and\ 2 \\[2em] \dfrac{sm_{max}}{\varphi_s + \theta_{fc}} - \left(\left(\dfrac{sm_t - sm}{\varphi_s}\right) + C_t\right) & , if\ between\ Conditions\ 2\ and\ 3 \end{cases} \quad ,$$
(3)

358

359 where SS is saturated storage in mm from the bottom of the soil, and sm is soil moisture (both

360 saturated and unsaturated storage) in the given time step in mm. Water table observations were

361 used to estimate SS from the field. Equation (3) is determined based on soil moisture curves in

362 Fig. 2 and water level *Conditions 1-3* discussed in Sect. 2.3.2. In Fig. 2, the first and second parts

363 of Eq. (3), which refer to *Conditions 1* to *2* and *2* to *3*, respectively, correspond to the volumes of

364 soil water highlighted in "blue" and "green."

365

366 *2.4.5 Lower semi-permeable soil layer and periodicity in annual groundwater levels*

367 This model application focused on the study site field without including other adjacent areas. This

368 was possible because years of field monitoring at this site have demonstrated that there is no

369 observable surface flow into the site from adjacent fields. The tile network is restricted to the field

370   and is not connected to tile drains or surface inlets in adjacent fields. However, field soil water

371   table observations show evidence of annual groundwater level periodicity/fluctuation (Rust et al.,

372   2019) that are sinusoidal in nature and cannot be neglected. Some studies predict the annual

373   groundwater oscillations or the annual responses of groundwater to precipitation by using sine and

374   cosine functions (De Ridder et al., 1974; Malzone et al., 2016; Qi et al., 2018). De Ridder et al.

375   (1974) studied the design of the drainage systems and described the seasonal groundwater

376   fluctuations observed in wells using sinusoidal curves. Malzone et al. (2016) used a sine function

377   to predict annual groundwater fluctuations in the hyporheic zone. Qi et al. (2018) and Rust et al

378   (2019) used a cross-wavelet transform, consisting of the superposition of sine and cosine curves,

379   to predict shallow groundwater response to precipitation at the basin scale. This approach, using

380   the sine function, was used in this application to simulate annual fluctuations in saturated storage,

381   in Eq. (4), over a period of 1 year, with minimums around the middle of the growing season (mid-

382   July), and maximums in the cold season (early February). This translates into the greater matric

383   potential, with soil moisture depletion, during the growing season, and lower matric potential, with

384   soil moisture increases, during the non-growing season, consistent with field observations. Thus,

385   a sine function representing the annual fluctuations in percolation rate from soil to groundwater

386   ($G_{y,i}$) layers in CRHM, through the lower soil semi-permeable layer (in mm hr^{-1}) is defined as:

387

388    $G_{y,i} = \left[A \times sin\left(\frac{(T_s - D_d \times 24) \times 360}{24 \times 365.25} \right) - B \right] \times f_{y,i}$ (4)

389

390   where T_s is the time step number, D_d is a time delay in days, A is the amplitude of the saturated

391   storage (SS) fluctuation, and B is an intercept factor. $f_{y,i}$ is a seasonal factor. The sine function

392   coefficient (D_d, A, and B) and seasonal factor were adjusted for the whole period and for each year

393 through model verification and shown in Table 1. Appendix C provides more details on the

394 implementation of Eq. (4). Although this is a simplification of the entire groundwater system

395 dynamics, it was needed here to provide a more controlled basis for testing the new module at the

396 field scale before expanding it to larger areas in future work.

397

398 *2.5   Model application and multi-variable, multi-metric validation*

399 The study site is a relatively small field, and 2 HRUs were sufficient to capture its hydrological

400 dynamics in CRHM. The HRUs represent (1) the area immediately upstream of the outlet where

401 surface ponding occurs (depression storage); and (2) the remaining field (Fig. 3). The maximum

402 ponding capacity of HRU 1 was estimated using the spatially distributed hydrodynamic model

403 FLUXOS-OVERFLOW (Costa et al., 2016, 2020b). The CRHM model with its new TDM module

404 was set up using the information described in Table 1. Soil textures at the LON site measured in a

405 25 m grid across three soil depths (0-25 cm, 25-50 cm, and 50-100 cm) averaged 29% sand, 48%

406 silt, and 23% clay (Ontario Ministry of Agriculture, Food and Rural Affairs Soil Team,

407 unpublished data). This soil grain size distribution corresponds with a soil-saturated hydraulic

408 conductivity of ~ 0.56 cm h^{-1} (~$10^{-2.5}$) (Garcia-Gutierrez et al., 2018), which was implemented

409 in CRHM (0.5 cm h^{-1}), corresponding to a field capacity of 0.04 (volumetric water content) and

410 h_{fc} of ~0.8 m (Twarskavi et al., 2009, based on a drainage flux of 0.1 cm d^{-1}).

411

412 A robust multi-variable, multi-metric model evaluation strategy was deployed to verify the

413 capacity of the model to predict tile flow and its impact on the local hydrology. The outflows

414 examined were tile flow, surface flow, and saturated storage. The multi-metric approach

415 contemplated five different methods, namely the Nash-Sutcliffe efficiency (*NSE*), Root-Mean-

416   Square Error (RMSE), Model Bias (Bias), Percentage Bias (Pbias), and RMSE-observation

417   standard deviation ratio (RSR). These methods were used to assess model accuracy. See Appendix

418   C for more details about the methodology used. It is generally assumed that $NSE>0.50$, $RSR \le$

419   0.70, and $PBias$ in the range of $\pm25\%$ are satisfactory for hydrological applications (Moriasi et

420   al., 2007). Five different metrics were used to evaluate model accuracy in order to describe

421   different aspects of the discrepancies between simulated and observed values. For example, Bias

422   reveals the positive or negative general deviations of simulated values from the observed values,

423   while RMSE shows the average absolute differences between them (Moriasi et al., 2007). Hourly

424   values were used in these calculations, which departs from the daily and monthly analyses typically

425   reported for these types of models. Although the hourly timestep is challenging for this sort of

426   simulation, it is an important advance forward toward more detailed, accurate, and advanced

427   models for tile-drained agricultural fields. For example, Costa et al., (2021) noted that the

428   successful extension of hydrological models to water quality studies relies on their ability to

429   operate at small time scales in order to capture intense, short-duration storms that may have a

430   disproportional impact on the runoff transport of some chemical species such as phosphorus – in

431   essence, to capture hot spots and hot moments for flux generation.

432

433   Table 1. Key model parameters in CRHM for representation of the LON site.

Model Parameter	Value	Unit	Adjusted/Calibrated	Comment
Soil depth or Soil thickness, T_{SL}	2	m	No	Assumed
Semipermeable layer depth	3	m	No	Assumed
Tile depth	0.9	m	No	Farmer/Blueprints of the field
Corn root depth	0.5	m	No	Online sources

Soil recharge zone thickness	0.5	m	No	Based on the root depth
Tile spacing	14	m	No	Farmer/Blueprints of the field
Soil porosity (soil drainable water) φ_S	0.045		Yes	Adjusted
Saturated Hydraulic conductivity, K_s in lower soil layer	5	mm h^{-1}	Yes	Adjusted
K_s in upper soil layer	5	mm h^{-1}	Yes	Adjusted
Capillary fringe thickness, T_{CF}	0.8	m	Yes	Adjusted
Capillary fringe drainable water, φ_C	0.03		Yes	Adjusted
Surface depression close to farm surface flow outlet (HRU2)	35	mm	Yes	Calculated
Surface depression in rest of the field (HRU1)	0	mm	No	Calculated
Surface area of HRU1	79000	m^2	No	Field observations and DEM
Surface area of HRU2	1000	m^2	No	Field observation and DEM
Soil module name in CRHM	WQ_soil		No	
Infiltration module name in CRHM	GreenAmpt		No	
Soil type in GreenAmpt module	5		Yes	Adjusted
Saturated K in GreenAmpt module	6	mm h^{-1}	Yes	Adjusted
Soil wilting point	0.025		Yes	Adjusted
A, in sine function	0.025	mm h^{-1}	Yes	Adjusted
B, in sine function	-0.005	mm h^{-1}	Yes	Adjusted
D_d, in sine function	15	d	Yes	Adjusted
$f_{2012,2}$ (Seasonal factor, sine function)	2.0		Yes	Adjusted
$f_{2015,2}$ (Seasonal factor, sine function)	1.8		Yes	Adjusted
$f_{2016,2}$ (Seasonal factor, sine function)	2		Yes	Adjusted

$f_{2017,2}$ (Seasonal factor, sine function)	1.4	Yes	Adjusted
$f_{y,i}$	1	No	By default for $y =$ 2012 to 2017 and $i = 1,2$

434

435

436

a) Schematic conceptual view of the CRHM model configuration, including soil layers, saturated storage (SS), groundwater, and tile flow.; and b) soil profile, including the capillary fringe and its location relative to the soil and tile.
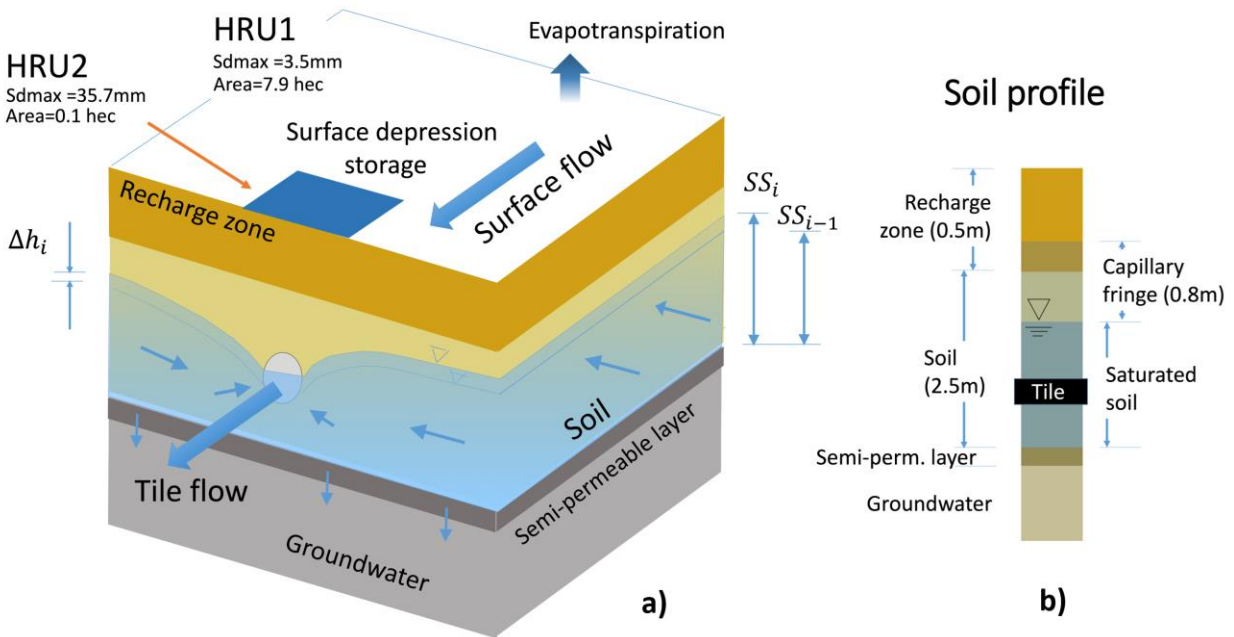
Figure 3.

437

438 Figure 3.   a) Schematic conceptual view of the CRHM model configuration, including soil layers, saturated storage (SS),

439 groundwater, and tile flow.; and b) soil profile, including the capillary fringe and its location relative to the soil and tile.

440

3.   Results

442 A multi-variable, multi-metric model evaluation approach was deployed to verify the capacity of

443 the model to predict not only tile flow but also the effects it has on the local hydrology, from

444 surface to sub-surface processes. The outflows examined were tile flow (Section 3.1), saturated

445 storage (Section 3.2), and surface flow (Section 3.3). The multi-metric approach contemplated five

446   different methods, namely the Nash-Sutcliffe efficiency (NSE), Root-Mean-Square Error (RMSE),

447   Model Bias (Bias), Percentage Bias (Pbias), and RMSE-observation standard deviation ratio

448   (RSR).

449   *3.1   Tile flow*

450   The model was able to capture most tile flow events, both in terms of the timing and magnitude of

451   peak flows and the most important seasonal patterns (Fig. 4). For example, the near absence of

452   flow during the growing season (May to September) was captured. The simulated flow peaks

453   generally had a good agreement with observations, as well as the low flow or base flows during

454   cold periods (December-March). The ascending and descending limbs of the response signal were

455   also adequately predicted.

456

457   Results show that tile flows generally occurred during snowmelt events, as indicated by the

458   synchrony between snow water equivalent (SWE) depletion and tile flow. The maximum

459   snowpacks (or snow water equivalent, SWE) were markedly smaller during the winters of 2016

460   and 2017 when compared with those of 2013 to 2015. However, this did not necessarily translate

461   into lower tile flows as precipitation also occurred as rain during these seasons. Although peak

462   tile drainage flow was not always predicted accurately, the model was able to capture the annual

463   trends of both an absence of tile flow during the summer months (growing season) and the

464   ascending and descending limbs of the tile hydrograph during events (Figure 4).

465

a)

467
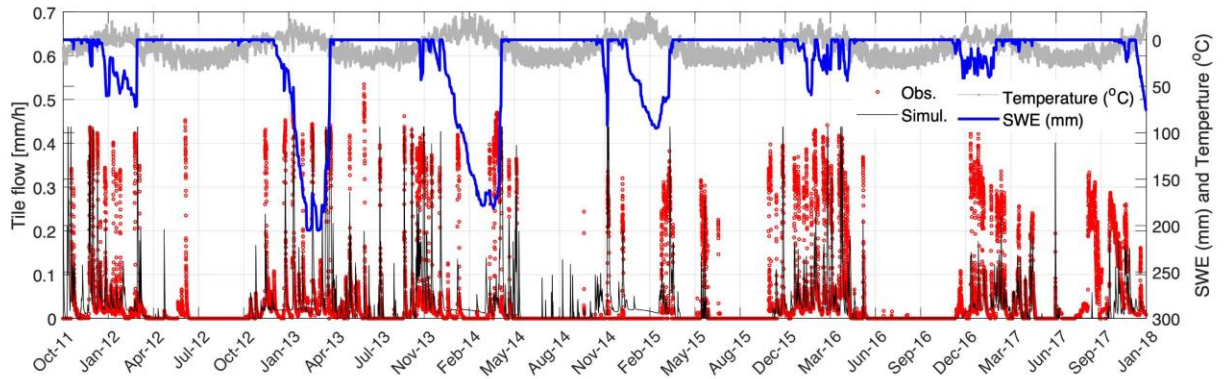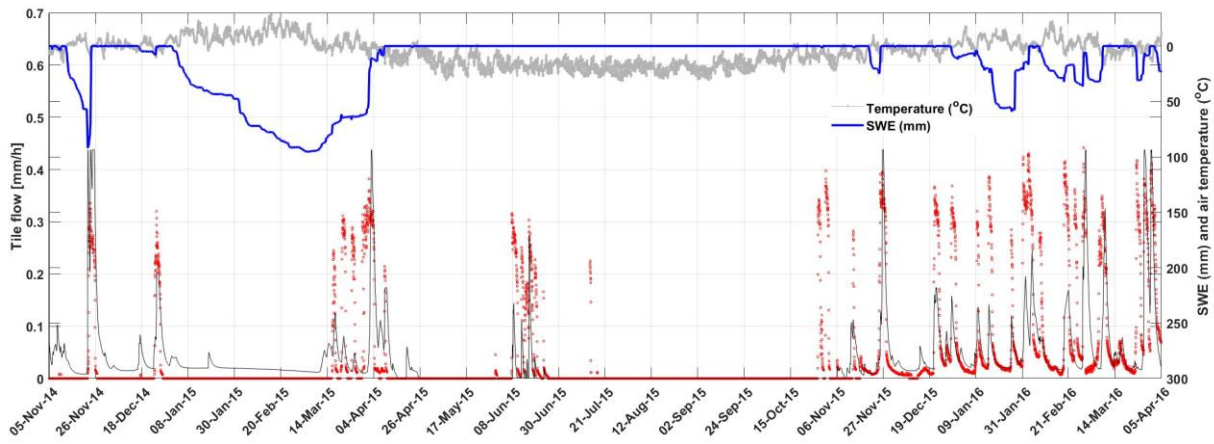
468   b)

Figure 4. Comparison between observed and simulated tile flows, simulated SWE (snow water equivalent), and observed air

temperature in the LON site, between October 2011 to January 2018 (a) and between November 2014 to April 2016 (b).

3.2   Soil saturated storage

Simulated and observed soil saturated storage are compared in Fig. 5, alongside air temperature

and precipitation observations. Despite the gaps in the observational record during two periodic

equipment failures, the model agrees well with observations. Above tile drains, fluctuations in

saturated storage were controlled by infiltration/recharge, tile flow, groundwater flow, and matric

potential that affect the drainable water from the capillary fringe. This caused flashier storage

478   responses above the tile that were captured well by the model. In contrast, tiles did not withdraw

479   water from the soil layer below the tile pipe and thus did not control fluctuations in saturated

480   storage when levels were below the drain pipe, and tile drains did not flow during such periods.

481   During the growing season, both the observed and simulated saturated storage dropped abruptly

482   because of the seasonal lowering of the regional groundwater water table. In the growing seasons

483   of 2012, 2015 and 2016, which were dry years, large declines in saturated storage were observed,

484   whereas in wetter years such as 2013 and 2014, seasonal saturated storage declines were smaller.

485   The seasonal declines in saturated storage during the growing season led to a cessation in tile flow

486   in most years (Fig. 4, 5), even following rainfall events. For example, there was a large

487   precipitation event (~35 mm) in the growing season of 2016 that did not produce tile flow (apparent

488   in both model and observations).
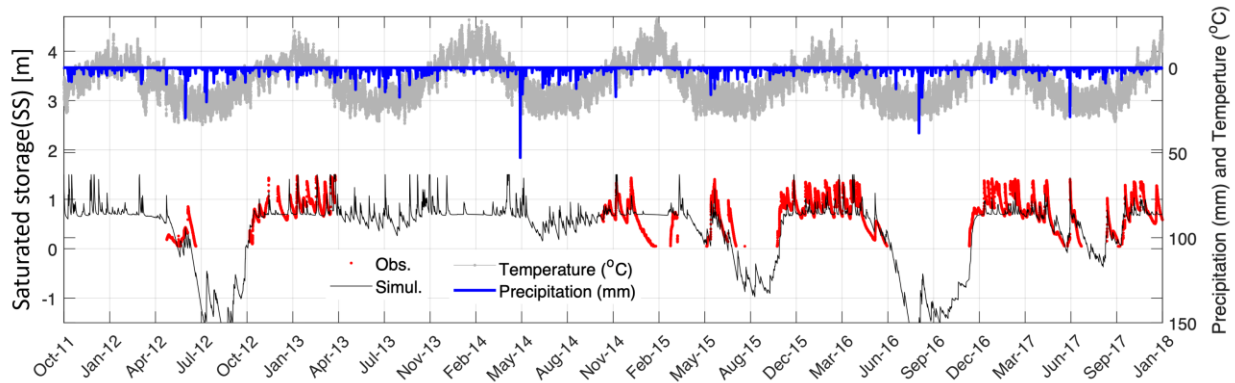
489

490   Figure 5. Time series of the simulated and observed saturated storage in the soil or groundwater layers of the model along with the

491   observed temperature and precipitation.

492

493   *3.3   Surface flow and total flow*

494   The model was not always able to capture the observed surface flow as satisfactorily as it captured

495   tile drainage (Fig. 6a). Some possible reasons are uncertainties in the measurements of surface

496   flow due to ponding in surface depressions on the field, which impeded the drainage of some of

497   the surface runoff prior to exiting the field through the culvert (see Fig. 1), or uncertainty in field

498   estimates of SWE. However, the model performance improved considerably when both runoff and

499   tile flow were combined (referred to as total flow, Fig. 6b). Indeed, most of the flow from the field

500   was through tile drains (80% in 5-year average) rather than surface runoff (20% in 5-year average,

501   Plach et al., 2019). The underestimation of both cumulative total and surface flows during 2017

502   and 2018 is possibly due to the removal of the blockage in the tile pipe in early 2017, which may

503   have affected both surface and tile flow. The differences in timing of the simulated and observed

504   surface flow for many of the main events (Figure 6) shows that there remain systematic issues in

505   simulation of surface flow by CRHM which should be addressed in future research.

(a)   (b)
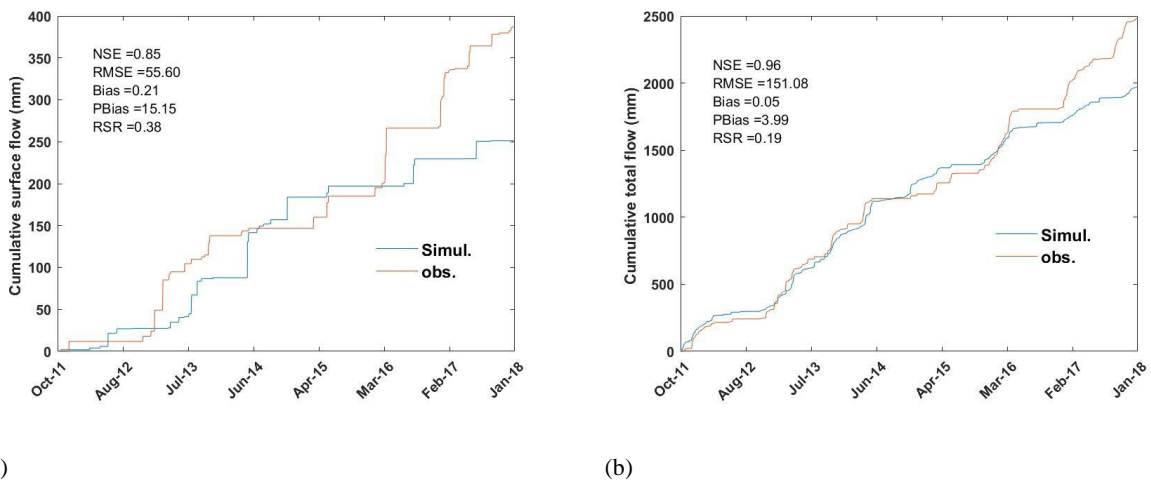
506   Figure 6. Observed and simulated cumulative surface flow (a) and total flow (b).

507

508   *3.4   Overall model performance*

509   The model performance was calculated based on hourly data for various model outputs (Table 2).

510   To compare the performance of the model in different seasons we calculated the coefficient for

511   entire year as well as separately for the growing and non-growing seasons. The results confirm

512   that the model is robust over an annual cycle in the sense that it can capture the main patterns of

513   tile flow, surface flow, and saturated storage. The Pbias values are below 25% for most of the

514   fluxes and cumulative fluxes. The RSR values are also generally below 1.0. The NSE values are

515   positive and above 0.3 for most fluxes, except for surface flow, where the model exhibited some

516   difficulties. The weaker performance of the model in the simulation of surface flow, which is

517   illustrated by the NSE coefficient, can be partly related to difficulties in measurement of surface

518   flow during flooding, ponding, and freeze-thaw on the surface. The performance coefficients were

519   calculated for the growing season, May-September (Table 2b) and non-growing season, October-

520   April (Table 2c). The results shows that surface flow biases are significantly larger and negative

521   in May-September and are smaller and positive during October-April. For tile flow the biases are

522   slightly higher in May-September whereas for saturated storage and total flow the biases are

523   slightly lower in May-September. The NSEs are more acceptable in October to April for surface

524   flow, tile flow and total flow, but the NSE for SS is more acceptable in May-September. The

525   overall performance of the model for both tile and surface flow is more reliable in the non-growing

526   season, when the regional water table was above the tile and saturated storage fluctuations were

527   mainly controlled by tile flow rather than regional groundwater oscillations.

528

529   Table 2. Performance coefficients for surface flow, tile flow and saturated storage (SS), as well as total (tile + surface) flow, for

530   the simulation period of October 2011 to January 2018. The coefficients were calculated for both hourly and daily flow rates, for

531   the whole year (a) for May to September (b) and for October to April (c). (Green and red color show the seasonal coefficients

532   improved and worsened, respectively, compared to their seasonal values).

533   a)   Coefficients for whole year

Performance coefficients	Surface flow	Tile flow	SS	Total flow	
NSE[*]	-2.29	0.31	0.49	-1.38	Coefficients calculated for hourly flow rates (mm h⁻¹)
RMSE[^]	0.27	0.08	0.26	0.30	
Bias[#]	0.54	0.24	0.14	0.28	
Pbias[$]	21.77	17.91	10.46	18.63	

27

RSR[&]	1.82	0.83	0.71	1.54	Coefficients calculated for daily flow rates (mm d⁻¹)
NSE	-0.73	0.29	0.50	0.01	
RMSE	2.04	1.72	0.24	2.92	
Bias	0.35	0.20	0.09	0.22	
Pbias	35.11	19.63	9.33	21.73	
RSR	1.31	0.84	0.70	0.99	

534

535

536   b) coefficients for May to September

Performance coefficients	Surface flow	Tile flow	SS	Total flow	
NSE[*]	-18.98	0.19	0.40	-11.76	Coefficients calculated for hourly flow rates (mm h⁻¹)
RMSE[^]	0.26	0.03	0.12	0.26	
Bias[#]	-1.43	0.49	0.03	0.11	
Pbias[$]	-142.79	48.88	3.44	10.96	
RSR[&]	2.85	0.57	0.39	2.27	
NSE	-3.89	0.21	0.41	-1.08	Coefficients calculated for daily flow rates (mm d⁻¹)
RMSE	1.39	0.73	0.11	1.66	
Bias	-1.43	0.49	0.02	0.11	
Pbias	-142.79	48.88	2.07	10.96	
RSR	1.41	0.56	0.39	0.92	

537

538   c) coefficients for October to April

Performance coefficients	Surface flow	Tile flow	SS	Total flow	
NSE[*]	-0.37	0.24	0.20	-0.04	Coefficients calculated for hourly flow rates (mm h⁻¹)
RMSE[^]	0.11	0.07	0.21	0.14	
Bias[#]	0.87	0.14	0.11	0.24	
Pbias[$]	86.59	13.56	11.00	24.11	
RSR[&]	0.90	0.67	0.77	0.79	
NSE	-0.11	0.26	0.24	0.18	Coefficients calculated for daily flow rates (mm d⁻¹)
RMSE	1.50	1.56	0.21	2.40	
Bias	0.87	0.14	0.11	0.24	
Pbias	86.59	13.56	10.58	24.11	

	RSR	0.81	0.67	0.75	0.70

539

540

541

542

543

544

545   *3.5   Presence of capillary fringe: effects and hypotheses*

546   Results show that the thickness and vertical positioning of the capillary fringe had a strong impact

547   on the amount of drainable soil water that flowed into the tiles. To investigate this effect further,

548   the response of tile flow and soil moisture to changes in the capillary fringe was examined. It

549   should be noted that although this thickness may change slightly depending on the soil type and

550   water retention curves (Skaggs et al., 1978), the model assumed a constant value given the field-

551   scale nature of the simulations and myriad of processes contemplated. However, despite the

552   simplification, the vertical positioning of the capillary fringe was still calculated and enabled a

553   dynamic (time-dependent) calculation of the drainable soil water that was available for tile

554   drainage over time.

555

556   *Effect of capillary fringe on tile flow*

557   Figure 7a relates the simulated normalized total cumulative tile flow (Q_{tR} , total tile flow divided

558   by the total tile flow when there is no influence of capillary fringe) to capillary fringe drainable

559   water ($\varphi_{cR} = \varphi_c/\varphi_s$) for two different φ_s values (0.045 and 0.125). The values were normalized

560   (0 – 1 scale) for comparison purposes. As expected, the model indicates that tile flow increases

561   with drainable water, but the relationship is non-linear, likely because as tile carrying capacity is

562   exceeded more frequently, there is more opportunity for groundwater seepage and

563   evapotranspiration. The direct effect of φ_s (comparing the solid and dashed lines) on tile flow is

564   small because the amount of water that can effectively drain to the tile is controlled by the capillary

565   fringe and the associated drainable soil water. Figure 7b looks at the impact of the capillary fringe

566   thickness on tile flow. Here, the values are also normalized. Results show that Q_{tR} decreases with

567   increasing normalized thickness of the capillary fringe, T_{CFR} ($\frac{T_{CF}}{D_t}$, capillary fringe thickness

568   divided by tile depth), but only while the T_{CFR} is less than 1 that is when the capillary fringe

569   position is above the tile but has not reached the soil surface. Beyond this point, increments in the

570   capillary fringe thickness have no impact on tile flow because *Condition 1* has been reached (see

571   Fig. 2), which essentially means that the capillary fringe has reached the soil surface. The match

572   between the curves for two different φ_s values shows that the changes in φ_s does not influence the

573   effect of normalized capillary fringe thickness and drainable water on normalized tile flow. In

574   Appendix D the sensitivity of cumulative tile flow and mean saturated storage to different

575   parameters are shown along with general approaches for evaluation of the model parameters for

576   new sites, the site with no tile flow and water table observations.

a)   b)
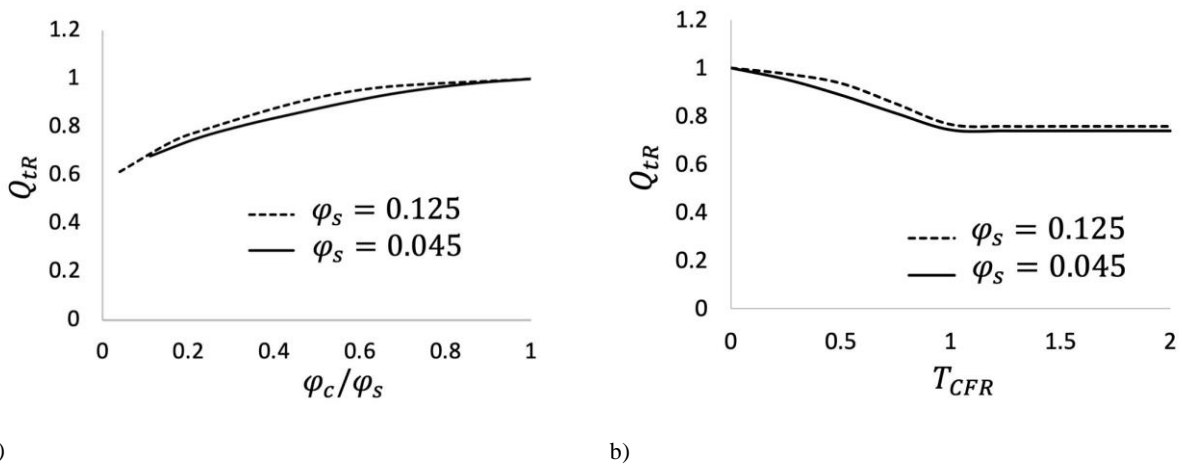
577   Figure 7. Comparison between normalized tile flow (Q_{tR}) and (a) normalized drainable soil water (φ_c/φ_s) and (b) capillary fringe

578   thickness (T_{CFR}) for different maximum soil saturation values (φ_s), by drawing the model prediction lines.

579

580   *Effect of capillary fringe on soil moisture*

581   Observations and simulations of saturated storage reveal a bimodal frequency distribution (Fig. 8

582   and 9, respectively) with peaks at 0.85 m and 1.25 m depth, with the former corresponding to the

583   influence of the tile pipe and the second peak reflecting that from the capillary fringe. I simulated

584   soil saturated storage frequency distributions (Fig. 9), show a first peak that highlights the

585   efficiency of the tile in removing soil moisture. In contrast, the second peak indicates a strong

586   model response to differences in the capillary fringe thickness. It shows that when there is near-

587   constant percolation from the bottom of the soil layer, the matric potential varies the greatest while

588   it remains between the tile depth and the soil surface. While the saturated storage fluctuates faster

589   and is more unstable within this range, it also remains there for shorter periods. This bimodal

590   response tends to push the saturated storage layer below the tile. In Figure 9, the first peak happens

591   at 0.9 m depth where the tile pipe is located, and the second peak happens at the depth equal to

592   capillary fringe thickness. In Figure 9 the second peak is clearer for the capillary fringe thickness

593   of more than 1000 mm. The first peak in the observed saturated storage frequency plot (Figure 8)

594   happened around 0.8 m which almost matches with the tile depth. And the second peak happened

595   at the depth of ~1.2 m which shows that the capillary fringe thickness should be around 1.2 m.

596   But, to have a more reliable estimate for the capillary fringe, based on Figure 8, data is needed at

597   depths greater than 1.5 m.

598

599   The bimodal behaviour of the observed and simulated saturated storage demonstrated here

600   provides the opportunity to quantify the thickness of the capillary fringe using continuously

601   monitored saturated storage. The capillary fringe thickness determined using this method can then

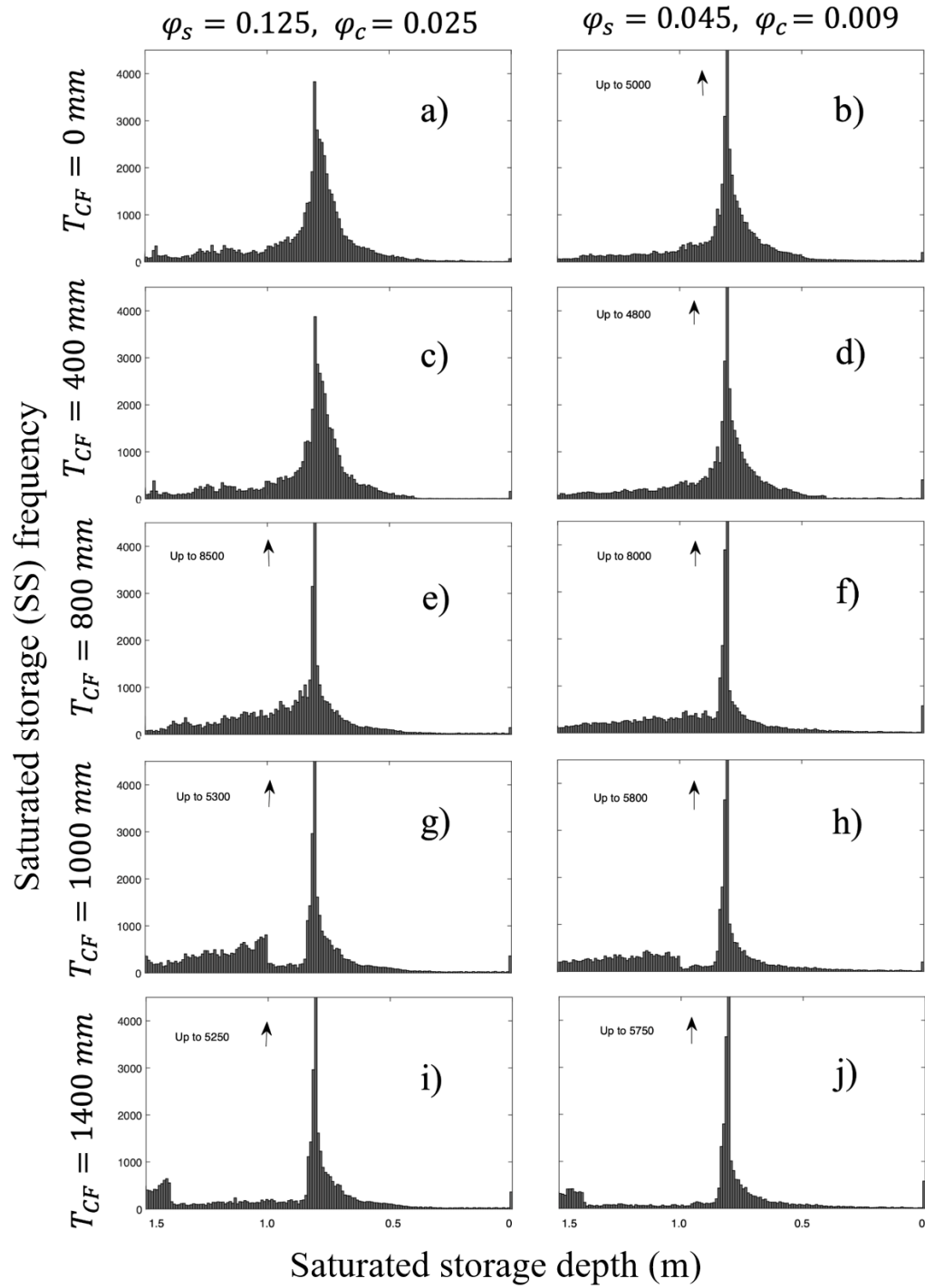602   be used as an input to the TDM module.
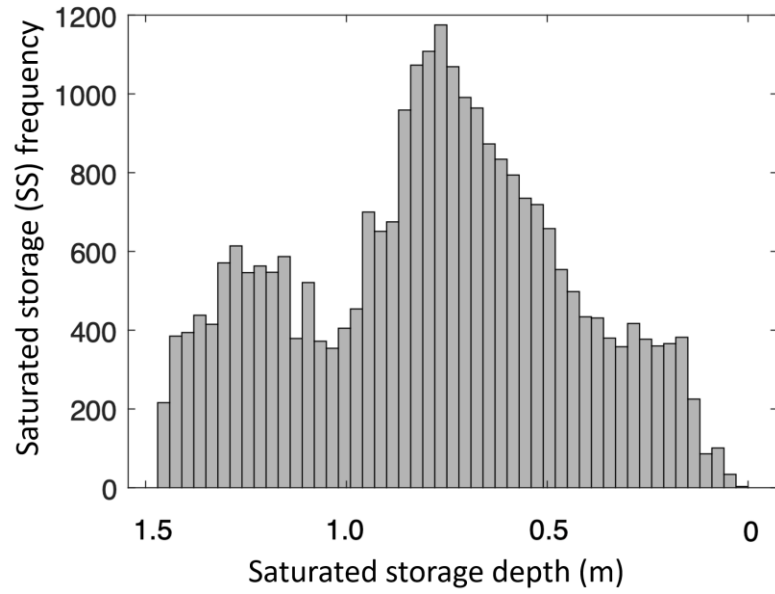
603

604   Figure 8. Histogram of the observed saturated storage distribution for the period pf 2011 to 2018 in LON (Londesborough).

605

Figure 9. Histograms of the simulated soil saturated storages versus saturated storage depth for the capillary fringe thicknesses of 0 (a,b), 400 (c,d), 800 (e,f), 1000 (g,h) and 1400 (I, j) mm and for the φ_s and φ_c of 0.125 and 0.025 (left column)as well as 0.045 and 0.009 (right column).

4.   Discussion

4.1   Insights into key control mechanisms of tile flow for model simulations

The model suggests that tile flow may not be accurately predicted exclusively based on the soil's

saturated storage and saturated hydraulic conductivity as suggested by the steady-state flow

assumptions of the Hooghoudt's equation (Hooghoudt, 1940). These results indicate two

additional controls: (1) the amount of drainable soil water in the soil, which has also been identified

in some field studies (*e.g.*, Skaggs et al., 1978; Moriasi et al., 2013) and (2) fluctuations in saturated

storage are important to account for in simulations. However, the relationship between drainable

water and tile flow rates is non-linear, as demonstrated in Fig. 7a. This is because the residence

time for groundwater seepage and evapotranspiration increases when the hydraulic tile carrying

capacity is exceeded. Comparatively, the effect of soil drainable water, φ_s (see also Fig. 7a) on tile

flow is small because the capillary fringe and associated drainable soil water control the amount

of water that can effectively flow to the tile.

The verification of the model also indicated that the slopes of the rising and falling limbs of tile

flow hydrographs and saturated storage were very sensitive to (1) the ratio between K_s and

drainable soil water; and (2) the net outflow in the soil through tile flow and fluctuations in

saturated storage. This is supported by previous studies showing rapid responses of tile flow to

precipitation events (Gentry et al., 2007; Smith et al., 2015) and others that have related rapid

responses in tile discharge to antecedent moisture conditions (Macrae et al., 2007; Vidon and

Cuadra, 2010; Lam et al., 2016a; Macrae et al., 2019), which can be affected by the development

of a capillary fringe and its non-drainable water.

634

635 Results show that large fluctuations in saturated storage and tile flow during the cold season, when

636 the water table tends to be above the tile, are primarily triggered by the development of a capillary

637 fringe that reduces the amount of drainable soil water. Model sensitivity tests showed that a small

638 amount of drainable soil water produces steeper rising and falling responses (and with larger

639 fluctuation amplitudes) in both the saturated storage and the tile flow. Indeed, this pattern can be

640 observed by exploring differences in tile drain responses in clay loam soils with larger field

641 capacities (and correspondingly smaller drainable water) and smaller hydraulic conductivity which

642 are more likely to experience pronounced oscillations (*e.g.*, steeper rising and falling response

643 curves) compared to tile drain responses of sandy soil, which is characterized by reduced capillary

644 forces, lower field capacities (but correspondingly larger drainable water) and higher hydraulic

645 conductivity. Notably, both model and observations of saturated storage reveal a bimodal (*i.e.*, two

646 peaks) frequency distribution when examined in relation to the tile depth and capillary fringe

647 thickness (Fig. 8 and 9, respectively). The two peaks (*i.e.* most frequently observed saturated

648 storage correspond with the (1) depth of the tile pipe (0.75 m), which demonstrates the efficacy of

649 the tile at rapidly removing excess soil water, and the (2) the capillary fringe thickness (for the

650 depths of 1.0 and 1.4 m, Figs. G, h, I and j) beyond which the amount of drainable water above the

651 water table significantly increases.

652

653 These findings align well with studies such as Lam et al. (2016a) that recorded soil moisture near

654 saturation after tile flow had ceased, suggesting the development of a capillary fringe. Combined

655 experimental and modeling works, such as in Moriasi et al. (2013) and Logsdon et al. (2010), also

656 discuss the impact of drainable soil water ("drainable porosity" or "specific water yield") on tile

657   flow and note that the drainable water is, in turn, dependent on the soil type, soil-water dynamic

658   and water table depth. However, these studies did not explore the dynamic nature of the capillary

659   fringe and its thickness relative to the soil column above in determining the transient amount of

660   drainage soil water that will impact the saturated storage frequency distribution and tile flow

661   differently over time (*Conditions 1* to *3*, see Fig. 2). Herein, while a capillary fringe with a fixed

662   thickness that is generally related to the soil properties was assumed, its vertical positioning was

663   simulated dynamically, which allowed determining the drainable soil water based on the evolution

664   of pressure head corresponding to field capacity. Thus, the development of the TDM has provided

665   a step forward in the modeling of tile drainage and suggests that in loam soils such as those at the

666   study site, the effects of a capillary fringe on tile flow should be included. Soil moisture (soil

667   unsaturated storage) measurements from the study site by Van Esbroeck et al., (2017) between

668   November 2011 and May 2014 from depths of 10, 30, and 50 cm (using EC-5 Soil Moisture Smart

669   Sensor) showed that almost 90% of the gravitational soil moisture drains out with 0.5 to 2.5 h.

670   This suggests that the saturated storage and capillary fringe can reach an equilibrium condition

671   within one hour at this field site, enabling the use of a steady state equation (Hooghoudt, 1940) to

672   predict the dynamic behaviour of the water table fluctuations.

673

674   *4.2   Importance of capturing seasonal patterns in saturated storage to improve tile flow*

675   *predictions*

676   The saturated storage changed dramatically between seasons affecting soil moisture (both

677   saturated and unsaturated storage in the soil) and tile flow patterns. Both observations and model

678   results show that low precipitation and higher evapotranspiration rates tend to produce little tile

679   flow during the growing season. These seasonal patterns in precipitation and evapotranspiration

680   are accompanied by a reduction in soil moisture (both unsaturated and saturated) that leads to a

681   substantial storage capacity in fields. Even following moderate and high-intensity storms during

682   the growing season, rapid soil moisture increases were observed (both saturated and unsaturated

683   soil storage); however, tile flow rarely developed due to higher evapotranspiration and a seasonal

684   decrease in the saturated storage , suggesting that the soil is able to hold the water (Lam et al.,

685   2016a; Van Esbroeck et al., 2016). In contrast, tile flow was often observed during the cold season,

686   with significantly smaller evapotranspiration fluxes, even during smaller rainfall-runoff and

687   snowmelt events because of reduced soil storage but also a seasonal increase in regional

688   groundwater table (Lam et al., 2016a; Macrae et al., 2007, 2019; Van Esbroeck et al., 2016). This

689   concurs with several studies throughout the Great Lakes and St. Lawrence region that have

690   reported stronger tile responses during the non-growing season, with the summer months often

691   showing little to no tile flow (Lam et al., 2016a, 2016b; Jamieson et al., 2003; Macrae et al., 2007;

692   Hirt et al., 2011; King et al., 2016; Van Esbroeck et al., 2016; Plach et al., 2019).

693   These results (the controlling effect of soil drainable water and saturated storage

694   fluctuations on tile flow) suggest that while soil moisture (both saturated and unsaturated storage)

695   is largely controlled by tile flow rather than saturated storage in the cold season, this reverses in

696   the growing season (*i.e.,* soil moisture controls tile flow), with soil moisture (both saturated and

697   unsaturated storage) being also impacted by evapotranspiration. The controlling effect of

698   groundwater fluctuations in the growing season has also been studied by Hansen et al., (2019).

699   The model indicated that the rapid drops in observed saturated storage during the growing season

700   could not be explained by evapotranspiration alone, thus pointing to the role of saturated storage.

701   Johnsen et al. (1995) and Akis (2016) also showed that the effect of groundwater accretion was

702   more effective on tile flows than surface runoff. Also, Vaughan et al. (1999) found that tile drain

703   flows in their study site in San Joaquin Valley of California were better explained and related to

704   nonlocal groundwater appearance than to local variations in irrigation amount, evapotranspiration,

705   variation in water storage or tile drain blockage. Thus, it was determined that in addition to soil

706   saturated hydraulic conductivity and soil thickness, the seasonal fluctuations in saturated storage

707   and capillary fringe drainable water are other important controlling factors on tile flow rates.

708

5.   Conclusions

710   A new tile drain module within the modular Cold Regions Hydrological Modelling (CRHM)

711   platform has been created and tested at the field scale to support the management of agricultural

712   basins with seasonal snow covers. The model was tested and validated for a small working farm

713   in southern Ontario, Canada, and presents a step forward in the dynamic simulation of tile flow

714   and its effects on the hydrological cycle in cold climates. Observations and model results showed

715   that the dynamic prediction of tile flow and soil moisture at catchment scales needs to account for

716   (1) the amount of drainable soil water that can be affected by the development of a capillary fringe

717   and (2) fluctuations in saturated storage, in addition to (3) the typical saturated storage near the tile

718   pipe depth,   and (4) the soil saturated hydraulic conductivity considered by the steady-state flow

719   Hooghoudt's equation. The saturated storage and matric potential changed dramatically between

720   seasons, affecting patterns of overall soil moisture and tile flow. Observations and model results

721   showed that low precipitation and higher evapotranspiration rates caused minimal tile flows during

722   the crop-growing season. Conversely, tile flow was often observed during the cold season, even

723   during small rainfall-runoff and snowmelt events, due to a seasonal increase in soil-saturated

724   storage.

725 Model sensitivity tests showed that the capillary fringe strongly affected the amount of drainable

726 soil water flowing into the tile. Tile flow increased with drainable water, but the relationship is

727 highly non-linear likely because, as the tile carrying capacity is exceeded more frequently, there is

728 more opportunity time for groundwater seepage and evapotranspiration. Finally, observations and

729 model results reveal a bimodal saturated storage response in the presence of tiles, which is

730 controlled by the relative positioning of the capillary fringe in relation to the soil surface and the

731 depth of tile drains below the soil surface. Capturing these dynamics is a critical advance enabling

732 the accurate prediction of the swift hydrological changes caused by the presence of tiles in models.

733 The TDM was developed as a first approximation from a single field site with the goal of providing

734 insight into control mechanisms of tile flow. Given this limitation, it is not yet widely applicable

735 across multiple field sites and for larger areas. Yet, the development of this module provides

736 critical insights into its potential and performance for hourly time-step simulations, as well as the

737 importance of saturated storage fluctuations and simplifying the capillary fringe parameters within

738 models in some landscape type. Future work should build on the current model adapting it to

739 different soil textures, such as those in clay loam soils, where preferential flow can have a strong

740 impact on -saturated storage and tile flow. Also, explicit representation of unsaturated flow may

741 be needed to enable the use of the model in regions where groundwater is disconnected from

742 surface water, as commonly happens in arid and semi-arid regions. Subsequent steps should

743 include also the integration of the new TDM model with CRHM's frozen soil and water quality

744 modules.

745

746 **Code/Data availability**

747   The tile flow and soil water table data are not publicly available and will be provided upon request

748   to the data owner, Merrin Macrae. TDM code is not completely implemented in the main version

749   of the Cold Regions Hydrological Model platform and is provided upon request to the

750   corresponding author.

751

Author contribution

753   MK and DC developed the new model code and performed the simulations. MM prepared the data

754   and supported the field work. JP developed CRHM. MK, DC and MM prepared the manuscript

755   with contributions from JP and RP. All authors edited the manuscript.

756

Competing interests

758   The contact author has declared that none of the authors has any competing interests.

759

769

References

770 **References**

771 Akis R.: Simulation of Tile Drain Flows in an Alluvial Clayey Soil Using HYDRUS 1D,

772 American-Eurasian J. Agric. & Environ. Sci., 16 (4), 801-813,

773 https://doi.org/10.5829/idosi.aejaes.2016.16.4.12906 , 2016.

774

775 Arheimer, B., Nilsson, J., and Lindstrom, G.: Experimenting with Coupled Hydro-Ecological

776 Models to Explore Measure Plans and Water Quality Goals in a Semi-Enclosed Swedish Bay,

777 Water, 7(7), 3906-3924, https://doi.org/10.3390/w7073906, 2015.

778

779 Arnold, J. G., Srinivasan, R., Muttiah, R. S., and Williams, J. R.: Large area hydrologic modeling

780 and assessment part I: model development, J. Am. Water. Resour. Assoc., 34, 73-89,

781 https://doi.org/10.1111/j.1752-1688.1998.tb05961.x, 1998.

782

783 Badr, A. W.: Physical properties of some North Carolina Organic Soils and the effect of land

784 development on these properties, M.S. Thesis, Department of Biological and Agricultural

785 Engineering, North Carolina State University, Raleigh, NC. 67 p., 1978.

786

787 Bleam, W. (2nd Edition): Soil and Environmental Chemistry, Academic Press, eBook ISBN:

788 9780128041956, 2017.

789

790

791   Brockley, R. P.: The effect of nutrient and moisture on soil nutrient availability, nutrient uptake,

792   tissue nutrient concentration, and growth of Douglas-Fir seedlings, Master Thesis, The University

793   of British Columbia, 1976.

794

795   Broughton, R. and Jutras, P.: Farm Drainage. In the Canadian Encyclopedia,

796   https://www.thecanadianencyclopedia.ca/en/article/farm-drainage/, last access: 14 February 2019,

797   2013.

798

799   Clark, M. P., Nijssen, B., Lundquist, J. D., Kavetski, D., Rupp, D. E., Woods, R. A., Freer, J. E.,

800   Gutmann, E. D., Wood, A. W., Brekke, L. D., Arnold, J. R., Gochis, D. J., & Rasmussen, R. M..

801   A unified approach for process-based hydrologic modeling: 1. Modeling concept. Water Resources

802   Research, 51(4), 2498–2514. https://doi.org/https://doi.org/10.1002/2015WR017198, 2015a.

803

804   Clark, M. P., Nijssen, B., Lundquist, J. D., Kavetski, D., Rupp, D. E., Woods, R. A., Freer, J. E.,

805   Gutmann, E. D., Wood, A. W., Gochis, D. J., Rasmussen, R. M., Tarboton, D. G., Mahat, V.,

806   Flerchinger, G. N., & Marks, D. G. A unified approach for process-based hydrologic modeling: 2.

807   Model implementation and case studies. Water Resources Research, 51(4), 2515–2542.

808   https://doi.org/https://doi.org/10.1002/2015WR017200, 2015b.

809

810   Coelho, B. B., Murray, R., Lapen, D., Topp, E., and Bruin, A.: Phosphorus and sediment loading

811   to surface waters from liquid swine manure application under different drainage and tillage

812   practices, Agric. Water Manag., 104, 51-61, https://doi.org/10.1016/j.agwat.2011.10.020, 2012.

813

814 Cordeiro, M. R. C. and Ranjan, R. S.: Corn yield response to drainage and subirrigation in the

815 Canadian Prairies, Trans. ASABE. 55(5), 1771-1780, https://doi.org/10.13031/2013.42369, 2012.

816

817 Cordeiro, M. R. C., Wilson, H. F., Vanrobaeys, J., Pomeroy, J. W., Fang, X., and The Red-

818 Assiniboine Project Biophysical Modeling Team: Simulating cold-region hydrology in an

819 intensively drained agricultural watershed in Manitoba, Canada, using the Cold Region

820 Hydrological Model, Hydrol. Earth Syst. Sci., 21, 3483-3506, https://doi.org/10.5194/hess-21-

821 3483-2017, 2017.

822

823 Correll, D.: The role of phosphorus in the eutrophication of receiving waters: a review, J. Environ.

824 Qual., 27, 261-266, https://doi.org/10.2134/jeq1998.00472425002700020004x, 1998.

825

826 Costa, D., Klenk, K., Knoben, W., Ireson, A., Spiteri, R. J., and Clark, M.: OpenWQ v.1: A multi-

827 chemistry modelling framework to enable flexible, transparent, interoperable, and reproducible

828 water quality simulations in existing hydro-models, EGUsphere [preprint],

829 https://doi.org/10.5194/egusphere-2023-2787, 2023.

830

831 Costa, D., Sutter, D., Shepherd, A., Jarvie, H., Wilson, H., Elliott, J., Liu, J., and Macrae, M.:

832 Impact of climate change on catchment nutrient dynamics: insights from around the

833 world. Environmental Reviews. **31**(1): 4-25. https://doi.org/10.1139/er-2021-0109, 2022

834

835 Costa, D., Baulch, H., Elliott, J., Pomeroy, J., and Wheater, H.: Modelling nutrient dynamics in

836 cold agricultural catchments: A review, Environ. Model. Softw., 124, 104586,

837 https://doi.org/10.1016/j.envsoft.2019.104586, 2020a.

838

839 Costa, D., Shook, K., Spence, C., Elliott, J., Baulch, H., Wilson, H., and Pomeroy, J.: Predicting

840 variable contributing areas, hydrological connectivity, and solute transport pathways for a

841 Canadian Prairie basin, Water Resour. Res., 56, 1-23, https://doi.org/10.1029/2020WR02798,

842 2020b.

843

844 Costa, D., Burlando, P., Liong, S.-Y.: Coupling spatially distributed river and groundwater

845 transport models to investigate contaminant dynamics at river corridor scales. Environmental

846 Modelling & Software, 86, 91–110. https://doi.org/10.1016/j.envsoft.2016.09.009, 2016.

847

848 Costa, D., Pomeroy, J. W., Brown, T., Baulch, H., Elliott, J., and Macrae, M.: Advances in the

849 simulation of nutrient dynamics in cold climate agricultural basins: Developing new nitrogen and

850 phosphorus modules for the Cold Regions Hydrological Modelling Platform, J. Hydrol., 603, 1-

851 17, https://doi.org/10.1016/j.jhydrol.2021.126901, 2021.

852

853

854 De Ridder, N. A., Takes, C. A. P., van Someren, C. L., Bos, M. G., Messemaeckers van de Graaff,

855 R. H., Bokkers, A. H. J., Stransky, J., Wiersma-Roche, M. F. L., and Beekman, T.: Drainage

856 Principles and Applications. International Institute for Lan Reclamation and Improvement, P.O.

857 Box 45 Wageningen The Netherlands, 1974.

858

859 Du, B., Arnold, J. G., Saleh, A., and Jaynes, D. B.: Development and application of SWAT to

860 landscapes with tiles and potholes, Trans. ASAE, 48, 1121-1133,

861 https://doi.org/10.13031/2013.18522, 2005.

862

863 Du, B., Saleh, A., Jaynes, D. B., and Arnold, J. G.: Evaluation of SWAT in simulating nitrate

864 nitrogen and atrazine fates in a watershed with tiles and potholes, Trans. ASABE, 49, 949-959,

865 https://doi.org/10.13031/2013.21746, 2006.

866

867 ECCC, Canadian Climate Normals 1981-2010 Station Data,

868 https://climate.weather.gc.ca/climate_normals/results_1981_2010_e.html?searchType=stnProx&

869 txtRadius=25&selCity=&selPark=&optProxType=custom&txtCentralLatDeg=43&txtCentralLat

870 Min=41&txtCentralLatSec=55&txtCentralLongDeg=81&txtCentralLongMin=28&txtCentralLon

871 gSec=47&txtLatDecDeg=&txtLongDecDeg=&stnID=4545&dispBack=0, last access: 5 February

872 2020.

873

874

875 Environment Canada, Canadian Climate Normals 1981-2010 Station Data,

876 https://climate.weather.gc.ca/climate_data/daily_data_e.html?hlyRange=%7C&dlyRange=1966-

877 06-01%7C2021-06-14&mlyRange=1966-01-01%7C2006-12-

878 01&StationID=4603&Prov=ON&urlExtension=_e.html&searchType=stnName&optLimit=year

879 Range&StartYear=1840&EndYear=2022&selRowPerPage=25&Line=0&searchMethod=contain

880   s&Month=6&Day=4&txtStationName=Wroxeter&timeframe=2&Year=2021, last access: 10

881   May 2020.

882

883   Fang, X., Pomeroy, J. W., Westbrook, C. J., Guo, X., Minke, A. G., and Brown, T.: Prediction of

884   snowmelt derived streamflow in a wetland dominated prairie basin, Hydrol. Erath Syst. Sci., 14,

885   991-1006, https://doi.org/10.5194/hess-14-991-2010, 2010.

886

887   Fang, X., Pomeroy, J. W., Ellis, C. R., MacDonald, M. K., DeBeer, C. M., and Brown, T.: Multi-

888   variable evaluation of hydrological model predictions for a headwater basin in the Canadian Rocky

889   Mountains, Hydrol. Earth Syst. Sci., 17, 1635-1659, https://doi.org/10.5194/hess-17-1635-2013,

890   2013.

891

892   Filippelli, G. M.: The global phosphorus cycle, Rev. Mineral. and Geochem., 48, 391-425,

893   https://doi.org/10.2138/rmg.2002.48.10, 2002.

894

895   Frey, S. K., Hwang, H. T., Park, Y. J., Hussain, S. I., Gottschall, N., Edwards, M., and Lapen, D.

896   R.: Dual permeability modeling of tile drain management influences on hydrologic and nutrient

897   transport characteristics in macroporous soil, J. Hydrol., 535, 392-406,

898   http://dx.doi.org/10.1016/j.jhydrol.2016.01.073, 2016.

899

900   Gentry, L. E., David, M. B., Royer, T. V., Mitchell, C. A., and Starks, K.: Phosphorus transport

901   pathways to streams in tile-drained agricultural watersheds, J. Environ. Quality., 36, 408-415,

902   https://doi.org/10.2134/jeq2006.0098, 2007.

903

904 Garcia-Gutierrez, C., Pachepsky, Y., and Martin, M. A.: Technical note: Saturated hydraulic

905 conductivity and textural heterogeneity of soils, Hydrol. Earth Syst. Sci., 22, 3923-3932,

906 https://doi.org/10.5194/hess-22-3923-2018, 2018.

907

908 Green, C. H., Tomer, M. D., Di Luzio, M., and Arnold, J. G.: Hydrologic evaluation of the Soil

909 and Water Assessment Tool for large tile-drained watershed in Iowa, Trans. ASABE., 49, 413-

910 422, https://doi.org/10.13031/2013.20415, 2006.

911

912 Hansen, A. L., Jakobsen, R., Refsgaard, J. C., Hojberg, A. L.,Iversen, B. V., and Kjaergaard, C.:

913 Groundwater dynamics and effect of tile drainage on water flow across the redox interface in a

914 Danish Weichsel till area, Advances in Water Resources, 123, 23-39,

915 https://doi.org/10.1016/j.advwatres.2018.10.022, 2019.

916

917 Hirt, U., Wetzig, A., Amatya, M. D., and Matranga, M.: Impact of seasonality on artificial drainage

918 discharge under temperate climate conditions, Int. Rev. Hydrobiol., 96, 561-577,

919 https://doi.org/10.1002/iroh.201111274, 2011.

920

921 Hooghoudt, S. B.: Bijdrage tot de kennis van enige natuurkundige grootheden van de grand.

922 Verslagen van Landbouwkundige Onderzoekingen, 46(7), 515-707, the Hague, The Netherlands

923 (in Dutch), 1940.

924

925   ICID: World Drained Area-2018. International Commission on Irrigation and Drainage.

926   http://www.icid.org/world-drained-area.pdf , last access: 14 February 2019.

927

928   Jamieson, A., Madramootoo, C. A., and Enright, P.: Phosphorus losses in surface and subsurface

929   runoff from a snowmelt event on an agricultural field in Quebec, Can. Biosyst. Eng., 45, 11-17,

930   2003.

931

932   Jarvie, H. P., Johnson, L. T., Sharpley, A. N., Smith, D. R., Baker, D. B., Bruulsema, T. W., and

933   Confesor, R.: Increased Soluble Phosphorus Loads to Lake Erie: Unintended Consequences of

934   Conservation Practices?, J. Environ. Qual., 46, 123-132, https://doi.org/10.2134/jeq2016.07.0248,

935   2017.

936

937   Javani-Jouni, H., Liaghat, A., Hassanoghli, A., and Henk, R.: Managing controlled drainage in

938   irrigated farmers' fields: A case study in the Moghan Plain, Iran, Agric. Water Manag., 208, 393-

939   405, https://doi.org/10.1016/j.agwat.2018.06.037, 2018.

940

941   Johnsen, K. E., Liu, H. H., Dane, J. H., Ahuja, L. R., and Workman, S. R.: Simulating Fluctuating

942   Water Tables and Tile Drainage with a Modified Root Zone Water Quality Model and a New

943   Model WAFLOWM, Transactions of the ASAE, 38 (1), 75-83,

944   https://doi.org/10.10031/2013.27814, 1995.

945

946   Kiesel, J., Fohrer, N., Schmalz, B., and White, M. J.: Incorporating landscape depressions and tile

947   drainages of a northern German lowland catchment into a semi-distributed model, Hydrol.

948   Process., 24, 1472-1486, https://doi.org/10.1002/hyp.7607, 2010.

949

950   King, K. W., Williams, M. R., Macrae, M. L., Fausey, N. R., Frankenberger, J., Smith, D. R.,

951   Kleinman, P. A. J., and Brown, L. C.: Phosphorus transport in agricultural subsurface drainage: A

952   review, J. Environ. Qual., 44(2), 467-485, https://doi.org/10.2134/jeq2014.04.0163, 2015.

953

954   King, K. W., Williams, M. R., and Fausey, N. R.: Effect of crop type and season on nutrient

955   leaching to tile drainage under a corn-soybean rotation, J. Soil and Water Conserv., 71, 56-68,

956   https://doi.org/10.2489/jswc.71.1.56, 2016.

957

958

959   Kladivko, E. J., Grochulska, J., Turco, R. F., Van Scoyoc, G. E., and Eigel, J. D.: Pesticide and

960   nitrate transport into subsurface tile drains of different spacings, J. Environ. Qual., 28, 997-1004,

961   https://doi.org/10.2134/jeq1999.00472425002800030033x, 1999.

962

963   Klaiber, L. B., Kramer, S. R., and Young, E. O.: Impacts of Tile Drainage on Phosphorus Losses

964   from Edge-of-field Plots in the Lake Champlain Basin of New York, Water, 12, 328,

965   https://doi.org/10.3390/w12020328, 2020.

966

967   Koch, S., Bauwe, A., and Lennartz, B.: Application of SWAT Model for a Tile-Drained Lowland

968   Catchment in North-Eastern Germany on Subbasin Scale, Water Resour. Manage., 27, 791-805,

969   https://doi.org/10.1007/s11269-012-0215-x, 2013.

970

971   Kokulan, V.: Environmental and Economic Consequences of Tile Drainage Systems in Canada,

972   The Canadian Agri-Food Policy Institute (CAPI), 2019.

973

974   Kokulan, V., Macrae, M. L., Ali, G. A., and Lobb, D. A.: Hydroclimatic controls on runoff

975   activation in a artificially drained, near-level vertisolic clay landscape in a Prairie climate, Hyrol.

976   Process., 33, 602-615, https://doi.org/10.1002/hyp.13347, 2019a.

977

978   Lam, W. V., Macrae, M. L., English, M. C., O'Halloran, I. P., Plach, J. M., and Wang, Y.: Seasonal

979   and event-based drives of runoff and phosphorus export through agricultural tile drains under

980   sandy loam soil in a cool temperate region, Hydrol. Process., 30, 2644-2656,

981   https://doi.org/10.1002/hyp.10871, 2016a.

982

983   Lam, W. V., Macrae, M. L., English, M. C., O'Halloran, I., and Wang, Y.: Effects of tillage

984   practices on phosphorus transport in tile drain effluent in sandy loam agricultural soils in Ontario,

985   Canada, J. Great Lakes Res., 42(6), 1260-1270, https://dx.doi.org/10.1016/j.jglr.2015.12.015,

986   2016b.

987

988

989   Lindstrom, G., Pers, C., Rosberg, J., Stromqvist, J., and Arheimer, B.: Development and testing of

990   the HYPE (Hydrological Predictions for the Environment) water quality model for different scales,

991   Hydrol. Res., 41(3-4), 295-319, https://doi.org/10.2166/nh.2010.007, 2010.

992

993   Logsdon, S. D., Schilling, K. E., Hernandez-Ramirez, G., Prueger, J. H., Hatfield, J. L., and Sauer,

994   T. J.: Field estimation of specific yield in a central Iowa crop field, Hydrol. Process., 24, 1369-

995   1377, https://doi.org/10.1002/hyp.7600, 2010.

996

997   Macrae, M. L., English, M. C., Schiff, S. L., and Stone, M. L.: Intra-annual variability in the

998   contribution of tile drains to basin discharge and phosphorus export in a first order agricultural

999   catchment, Agric. Water Manag., 92, 171-182, https://doi.org/10.1016/j.agwat.2007.05.015, 2007.

1000

1001   Macrae, M. L., Ali, G. A., King, K. W., Plach, J. M., Pluer, W. T., Williams, M., Morison, M. Q.,

1002   and Tang, W.: Evaluating Hydrologic Response in Tile-Drained Landscapes: Implications for

1003   Phosphorus   Transport,   J.   Environ.   Qual.,   48(5),   1347-1355,

1004   https://doi.org/10.2134/jeq2019.02.0060, 2019.

1005

1006   Malzone, J. M., Lowry, C. S., and Ward, A. S.: Response of the hyporheic zone to transient

1007   groundwater fluctuations on the annual and storm event time scales, Water Resour. Res., 52, 5301-

1008   5321, https://doi.org/10.1002/2015WR018056, 2016.

1009

1010   Mizukami, N., Clark, M. P., Sampson, K., Nijssen, B., Mao, Y., McMillan, H., Viger, R. J.,

1011   Markstrom, S. L., Hay, L. E., Woods, R., Arnold, J. R., & Brekke, L. D.. mizuRoute version 1: A

river network routing tool for a continental domain water resources applications. Geoscientific

Model Development, 9, 2223–2238. https://doi.org/10.5194/gmd-9-2223-2016 , 2016.

Moriasi, D. N., Arnold, J. G., Van Liew, M. W., Bingner, R. L., Harmel, R. D., and Veith, T. L.:

Model Evaluation Guidelines for Systematic Quantification of Accuracy in Watershed

Simulations, Trans. ASABE, 50(3), 885-900, https://doi.org/10.13031/2013.23153, 2007.

Moriasi, D. N., Gowda, P. H., Arnold, J. G., Mulla, D. J., Ale, S., Steiner, J. L., and Tomer, M. D.:

Evaluation of the Hooghoudt and Kirkham Tile Drain Equations in the Soil and Water Assessment

Tool to Simulate Tile Flow and Nitrate-Nitrogen, J. Environ. Qual., 42, 1699-1710,

https://doi.org/10.2134/jeq2013.01.0018, 2013.

OMAFRA: Tile Drainage Area, Government of Ontario, Canada, available at

https://geohub.lio.gov.on.ca/datasets/ontarioca11::tile-drainage-area/explore?showTable=true ,

2023.

Plach, J. M., Macrae, M. L., Ali, G. A., Brunke, R. R., English, M. C., Ferguson, G., Lam, W. V.,

Lozier, T. M., McKague, K., O'Halloran, I. P., Opolko, G., and Van Esbroeck, C. J.: Supply and

Transport Limitations on Phosphorus Losses from Agricultural Fields in the Lower Great Lakes

Region, Canada, J. Environ. Qual., 47, 96-105, https://doi.org/10.2134/jeq2017.06.0234, 2018a.

Plach, J. M., Macrae, M. L., Williams, M. R., Lee, B. D., and King, K. W.: Dominant glacial

landforms of the lower Great Lakes region exhibit different soil phosphorus chemistry and

1035   potential risk for phosphorus loss, J. Great Lakes Res., 44, 1057-1067,

1036   https://doi.org/10/1016/j.jglr.2018.07.005, 2018b.

1037

1038   Plach, J., Pluer, W., Macrae, M., Kompanizare, M., McKague, K., Carlow, R., and Brunke, R.:

1039   Agricultural Edge of Field Phosphorus Losses in Ontario, Canada: Importance of the Nongrowing

1040   Season in Cold Regions, J. Environ. Qual., 48, 813-821, https://doi.org/10.2134/jeq2018.11.0418,

1041   2019.

1042

1043   Pluer, W. T., Macrae, M., Buckley, A., and Reid, K.: Contribution of preferential flow to tile

1044   drainage varies spatially and temporally, Vadose Zone J., 19: e20043,

1045   https://doi.org/10.1002/vzj2.20043, 2020.

1046

1047   Pomeroy, J. W., Gray, D. M., Shook, K. R., Toth, B., Essery, R. L. H., Pietroniro, A., and

1048   Hedstrom, N. R.: An evaluation of snow accumulation and ablation processes for land surface

1049   modelling, Hydrol. Process., 12, 2339-2367, https://doi.org/10.1002/(SICI)1099-

1050   1085(199812)12:15, 1998.

1051

1052   Pomeroy, J. W., Gray, D. M., Brown, T., Hedstrom, N. R., Quinton, W. L., Granger, R. J., and

1053   Carey, S. K.: The cold regions hydrological model: a platform for basing process representation

1054   and model structure on physical evidence, Hydrol. Process., 21, 2650-2667,

1055   https://doi.org/10.1002/hyp.6787, 2007.

1056

Pomeroy, J. W., Fang, X., Shook, K., and Whitfield, P. H.: Predicting in Ungauged Basins Using Physical Principles Obtained Using the Deductive, Inductive, and Abductive Reasoning Approach, https://research-groups.usask.ca/hydrology/documents/pubs/papers/pomeroy_et_al_2003_3.pdf , 2013.

Pomeroy, J. W., Fang, X., and Marks, D. G.: The cold rain-on-snow event of June 2013 in the Canadian Rockies - characteristics and diagnosis, Hydrol. Process., 30, 2899-2914, https://doi.org/10.1002/hyp.10905, 2016.

Pomeroy, J. W., Brown, T., Fang, X., Shook, K. R., Pradhananga, D., Armstrong, R., Harder, P., Marsh, C., Costa, D., Krogh, S. A., Aubry-Wake, C., Annand, H., Lawford, P., He, Z., Kompanizare, M., and Lopez Moreno, J. I.: The cold regions hydrological modelling platform for hydrological diagnosis and prediction based on process understanding, J. of Hydrol., 615 (A), 128711, https://doi.org/10.1016/j.jhydrol.2022.128711, 2022.

Qi, P., Zhang, G., Xu, Y. J., Wang, L., Ding, C., and Cheng, C.: Assessing the Influence of Precipitation on Shallow Groundwater Table Response Using Combination of Singular Value Decomposition and Cross-Wavelet Approaches, Water, 10, 598, https://doi.org/10.3390/w10050598, 2018.

Quinton, J. G., Govers, G., van Oost, K., and Bardgett, R.: The impact of agricultural soil erosion on biochemical cycling, Nat. Geosci., 3, 311-314, https://doi.org/10.1038/ngeo838, 2010.

Raats, P. A. C. and Gardner, W. R.: Movement of water in saturated zone near a water table. Ch. 13 in Drainage for agriculture, J. van Schilfgraade, Ed., Agronomy Monograph. No. 17, American Society of Agronomy, Madison, WI, pp. 331-357, 1974.

Radcliffe, D. E., Reid, D. K., Blomback, K., Bolster, C. H., Collick, A. S., Easton, Z. M., Francesconi, W., Fuka, D. R., Johnsson, H., King, K., Larsbo, M., Youssef, M. A., Mulkey, A. S., Nelson, N. O., Persson, K., Ramirez-Avila, J. J., Schmieder, F., and Smith, D. R.: Applicability of Models to Predict Phosphorus Losses in Drained Fields: A Review, J. Environ. Qual., 44, 614-628, https://doi.org/10.2134/jeq2014.05.0220, 2015.

Rahman, M. M., Lin, Z., Jia, X., Steele, D. D., and DeSutter, T. M.: Impact of subsurface drainage on streamflows in Red River of the North basin, J. Hydrol., 511, 474-483, https://doi.org/10.1016/j.jhydrol.2014.01.070, 2014.

Refsgaard, J. C. and Storm, B.: MIKE SHE. In: Singh VP (ed) Computer models of watershed hydrology, Highlands Ranch, Water Research Pub, Colorado, 1995.

Richards L. A.: Capillary conduction of liquids through porous medium, Physics, 1 (5): 318-333, Bibcode:1931Physi…1..318R. https://doi.org/10.1063/1.1745010, 1931.

Rozemeijer, J. C., Visser, A., Borren, W., Winegram, M., van der Velde, Y., Klein, J., and Broers, H. P.: High-frequency monitoring of water fluxes and nutrient loads to assess the effects of

controlled drainage on water storage and nutrient transport, Hydrol. Earth Syst. Sci., 20, 347-358, https://doi.org/10.5194/hess-20-347-2016, 2016.

Rust, W., Holman, I., Bloomfield, J. Cuthbert, M., and Corstanje, R.: Understanding the potential of climate teleconnections to project future groundwater drought, Hydrol. Earth Syst. Sci., 23, 3233-3245, https://doi.org/10.5194/hess-23-3233-2019, 2019.

Ruttenberg, K.: The global phosphorus cycle. In Biochemistry, Vol. 8, treatiseon geochemistry, Schlesinger W (ed) (eds. H. Holland and K. Turekian). Elsevier-Pergamon: Oxford; 585-643, 2005.

Searcy, J. and Hardison, C. H.: Double –Mass Curves. Manual of Hydrology: Part 1, General Surface-Water Techniques, Geological Survey Water-Supply Paper 1541-B, 1960.

Schindler, D. W.: Recent advances in the understanding and management of eutrophication, Limnol. Oceanogr., 51, 356-363, https://doi.org/10.4319/lo.2006.51.1_part_2.0356, 2006.

Sharpley, A. N., Hedley, M. J., Sibbesen, E., Hillbricht-Ilkowska, A., House, W. A., and Ryszkowski, L.: Phosphorus transfer from terrestrial to aquatic ecosystems, In Phosphorus in the global environment, Tiessen H (ed), Scientific Committee on Problems of the Environment (SCOPE). John Wiley & SonsLtd.: Chichester; 171-199, 1995.

1124 Simunek J., van Genuchten M. Th., and Sejna M.: The HYDRUS Software Package for Simulating

1125 Two- and Three-Dimensional Moovement of Water, Heat and Multiple Solutes in Variably-

1126 Saturated Media, Technical Manual, Version 2.0, PC Progress, Prague, Czech Republic, pp. 258,

1127 2011.

1128

1129 Skaggs, R. W.: A water management model for shallow water table soils, University of North

1130 Carolina, Water Resource Research Institute, Technical Report 134, 1978.

1131

1132 Skaggs, R. W.: Combination surface-subsurface drainage systems for humid regions. J. Irrig.

1133 Drain. Div., ASCE. 106(IR4), 265-283, 1980a.

1134

1135 Skaggs, R. W.: Drainmod Reference Report, Methods for Design and Evaluation of Drainage-

1136 Water Management Systems for Soils with High Water Tables, U.S. Department of Agriculture,

1137 Soil Conservation Service, North Carolina State University, Raleigh, North Carolina, 1980b.

1138

1139 Skaggs, R. W., Wells, L. G., and Ghate, S. R.: Predicted and measured drainable porosities for

1140 field soils, Trans. ASAE, 21(3), 522-528, https://uknowledge.uky.edu/bae_facpub/199, 1978.

1141

1142 Skaggs, R. W., Youssef, M. A., and Chescheir, G. M.: DRAINMOD: Model Use, Calibration, and

1143 Validation, Trans. ASABE, 55(4), 1509-1522, https://doi.org/10.13031/2013.42259, 2012.

1144

1145 Smedema, L. K., Vlotman, W. F., and Rycroft, D.: Modern land Drainage. Planning, design and

1146 management of agricultural drainage systems, London: Taylor &Francis.

1147 https://doi.org/10.1201/9781003, 2004.

1148

1149 Smith, D. R., King, K. W., Johnson, L, Francesconi, W., Richards, P., Baker, D., and Sharpley,

1150 A. N.: Surface runoff and tile drainage transport of phosphorus in the Midwestern United States,

1151 J. Environ. Qual., 44, 495-502, https://doi.org/10.2134/jeq2014.04.0176, 2015.

1152

1153 Tomer, M. D., Meek, D. W., Jaynes, D. B., and Hatfield, J. L.: Evaluation of nitrate nitrogen fluxes

1154 from a tile-drained watershed in Central Iowa, J. Environ. Qual., 32, 642-653,

1155 https://doi.org/10.2134/jeq2003.6420, 2003.

1156

1157 Twarakavi, N. K. C., Sakai, M., and Simunek, J.: An objective analysis of the dynamic nature of

1158 field capacity, Water Resour. Res., 45, W10410, https://doi.org/10.1029/2009WR007944, 2009.

1159

1160 Van Esbroeck, C. J., Macrae, M. L., Brunke, R. I., and McKague, K.: Annual and seasonal

1161 phosphorus export in surface runoff and tile drainage from agricultural fields with cold temperate

1162 climates, J. Great Lakes Res., 42(6), 1271-1280, https://doi.org/10.1016/j.jglr.2015.12.014, 2016.

1163

1164 Van Esbroeck, C. J., Macrae, M. L., Brunke, R. R., and McKague, K.: Surface and subsurface

1165 phosphorus export from agricultural fields during peak flow events over the nongrowing season in

1166 regions with cool, temperate climates, Journal of Soil and Water Conservation, 72(1), 65-76,

1167 https://doi:10.2489/jswc.72.1.65 , 2017.

Vaughan, P. J., Suarez, D. L., Simunek, J., Corwin, D. L., and Rhoades, J. D.: Role of Groundwater Flow in Tile Drain Discharge, J. Environ. Qual., 28, 403-410, https://doi.org/10.2134/jeq1999.00472425002800020006x, 1999.

Vidon, P. and Cuadra, P. E.: Impact of precipitation characteristics on soil hydrology in tile drained landscapes, Hydrol. Process., 24, 1821-1833, https://doi.org/10.1002/hyp.7627, 2010.

Vivekananthan, K.: Environmental and Economic Consequences of Tile Drainage Systems in Canada, The Canadian Agri-Food Policy Institute, www.capi-icpa.ca, 2019.

Vivekananthan, K., Macrae, M., Lobb, D. A., and Ali, G. A.: Contribution of overland and tile flow to runoff and nutrient losses from vertisols in Manitoba, Canada, J. Environ. Qual., 48(4), 959-965, https://doi.org/10.2134/jeq2019.03.0103, 2019.

Waichler, S. R. and Wigmosta, M. S.: Development of Hourly Meteorological Values from Daily Data and Significance to Hydrological Modeling at H. J. Andrews Experimental Forest, Am. Meteorol. Soc., 4, 251-263, https://doi.org/10.1175/1525-7541(2003)4<251:DOHMVF>2.0.CO;2, 2003.

1189 Williams, M. R., King, K. W., and Fausey, N. R.: Drainage water management effects on tile

1190 discharge and water quality, Agric. Water Manag., 148, 43-51,

1191 http://dx.doi.org/10.1016/j.agwat.2014.09.017, 2015.

1192

1193 Williams, M. R., King, K. W., Ford, W., Buda, A. R., and Kennedy, C. D.: Effect of tillage on

1194 macropore flow and phosphorus transport to tile drains, Water Resour. Res., 52, 2868-2882,

1195 https://doi.org/10.1002/2015WR017650, 2016.

1196

1197 Williams, M. R., Livingston, S. J., Heathman, G. C., and McAfee, S. J.: Thresholds for run-off

1198 generation in a drained closed depression, Hydrol. Process., 1-14,

1199 https://doi.org/10.1002/hyp.13477, 2019.

1200

1201 Youngs, E. G.: Effect of the Capillary fringe on Steady-State Water Tables in drained Lands, J.

1202 Irrig. Drain. Eng., 138(9), 809-814, https://doi.org/10.1061/(ASCE)IR.1943-4774.0000467, 2012.

1203

1204

1205 **Appendix A**

1206 Table A1. Instrument names and descriptions

Instrument name	Description
Hach Flo-tote and FL900 logger	Flow velocity and water level measurement
U20, Onset Ltd.	Barometrically-corrected pressure transducer
Temperature Smart Sensor S-THB-M002	Air temperature measurement
Wind Smart Sensor S-WSET-M002	Wind speed measurement

(Silicon Pyranometer)-S-LIB-M003	Solar radiation sensor
Tipping bucketrain gauge, 0.2 mm Rainfall Smart Sensor – SRGB-M002	Rainfall measurement
RH Smart Sensor(S-THB-M002)	Relative Humidity measurement

1207

1208

1209

Appendix B

Table B1. Parameter names and their symbols in CRHM platform

Parameter symbol	Parameter name
Tair	Air temperature
Wspeed	Wind speed
RH	Relative Humidity
Qsi	Incoming solar irradiance
R	Rainfall
WQ_soil	Water Quality soil module
WT	Water table elevation above the semipermeable layer
SS	Soil saturated storage or the saturated part of the soil moisture
soil_moist	Soil moisture
Poro_soil	Soil porosity
AL	Above layer
BL	Below layer
K_s	Saturated hydraulic conductivity

1212

1213

1214

1215 **Appendix C**

1216

1217 Here, it was shown how seasonal factors ($f_{y,i}$) is assessed for different years. Equation (4) can be

1218 written as:

1219

1220 $$G_{y,i} = G \times f_{y,i}$$ (C1)

1221

1222 For each year (y), $f_{y,i}$ for the first ($f_{y,1}$) and second ($f_{y,2}$) part of the sine function (G) were

1223 assessed individually. It should be note that in first and second part of the sine function for each

1224 year G is larger than zero ($G \geq 0$) and smaller than zero ($G < 0$), respectively. G can be defined

1225 for the two parts as:

1226

1227 $$\begin{cases} if\ G \geq 0\ [i = 1\,]then\ f_{y,1} = x \\ if\ G < 0\ [i = 2\,]then\ f_{y,2} = y \end{cases}$$ (C-2)

1228

1229 G is the sine function representing the annual fluctuations in saturated storage (SS) or it can be

1230 simply defined as the percolation rate (in mm hr^{-1}) of soil water to groundwater through lower

1231 semi-permeable layer. So, for n years there are $n \times 2$ $f_{y,i}$ values. The default values for $f_{y,i}$ are 1

1232 and the default values can be changed for each year and for first and second parts in each year

1233 independently. Calculated $G_{y,i}$ in each time step add or subtracted to or from the total soil moisture

1234   depend on its sign. The $f_{y,i}$ values for the sine function parameters are presented in Fig. C1. The

1235   verified sine function time series along with time series of temperature, precipitation and

1236   calculated evapotranspiration are shown in Fig. C1. In this figure it is obvious that in years 2012

1237   and 2015 to 2017 the warm season amplitudes are larger. The ET values are happened more in the

1238   warm seasons (growing seasons). Also, the seasonal oscillation in sine function is very similar to

1239   the temperature general oscillations.
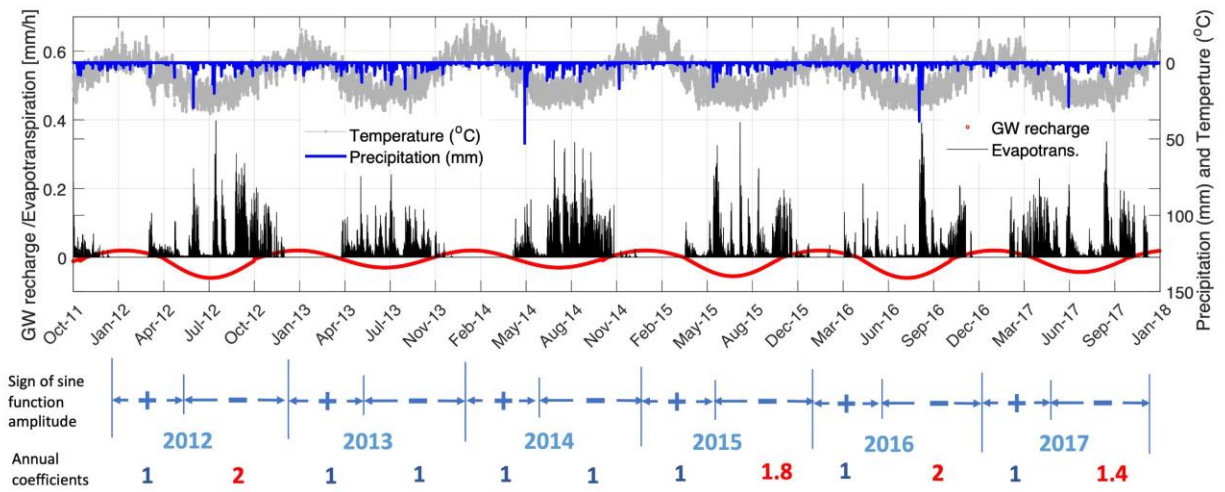
1240

1241   Figure C1. Time series of the adjustable sine function along with the time serioes of calculated evapotranspiration, temperature and

1242   precipitation during the study period from Oct 2011 to Sept 2018.

1243

1244

1245   **Appendix D**

1246   A sensitivity analysis was conducted for the cumulative tile flow (Q_{tc}), mean soil saturated storage

1247   (SS) (it is equal to water table elevation, WT , as it is mentioned in Eq. 3) and cumulative outflow

1248   rate from the semi-permeable layer at the bottom of the soil to groundwater (G_c) (see section 2.4.5,

1249   Eq. 4) with respect to six module parameters. Additionally, an approach for assessing model

1250   parameters at a new sites, potentially lacking water table elevation and tile flow observations is

1251   proposed.

1252

D.1 Sensitivity analysis

1253

1254 In this section, the sensitivity of Q_{tc}, SS and G_c to six distinct module parameters, namely capillary

1255 fringe thickness (T_{CF}), capillary fringe drainable water (φ_c), soil saturated hydraulic conductivity

1256 (K), soil thickness (T_{SL}), sine function amplitude (A) and sine function (B) was examined. Q_{tc}, G_c

1257 and SS were computed over the entire simulation period, expressed in units of mm, mm and m,

1258 respectively. Figures D-1a to f illustrate these sensitivities, with each parameter's impact discussed

1259 in dedicated sections.
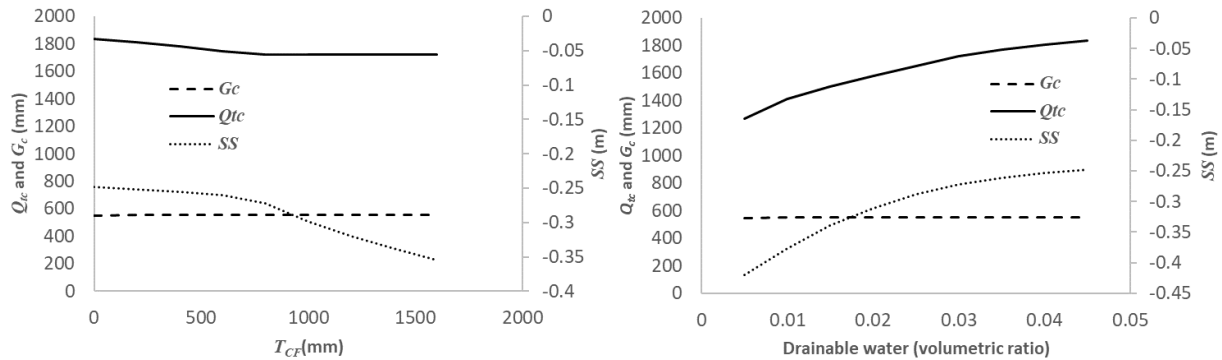
1260

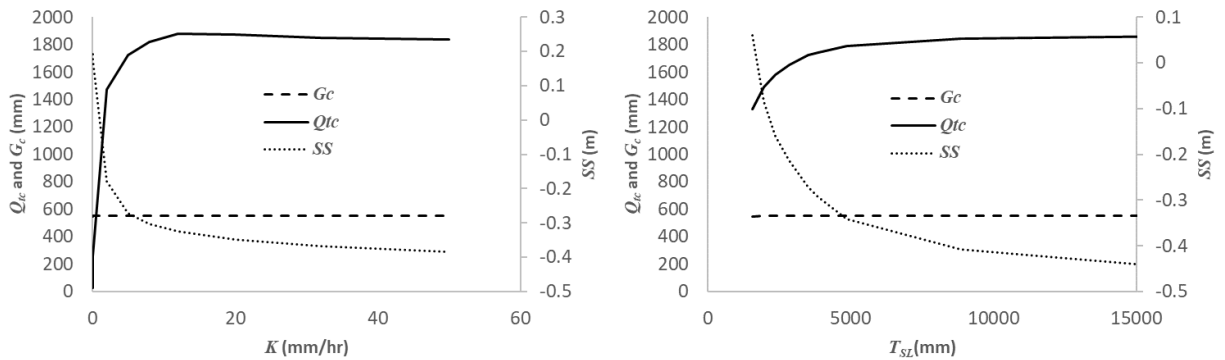1261   a)   b)

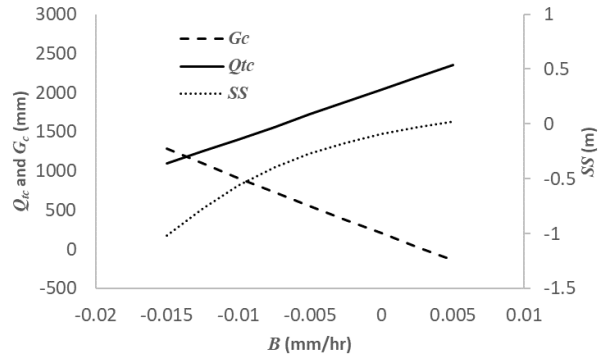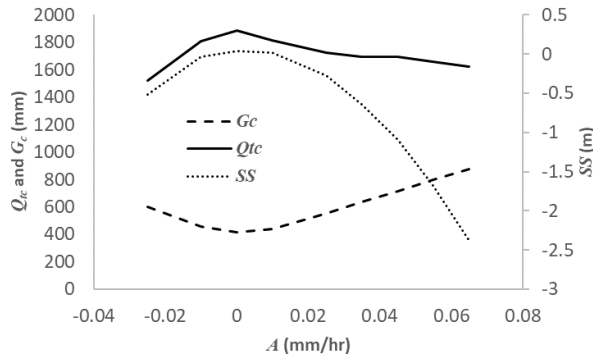1262

1263   c)   d)

1264

1265   e)   f)

1266   Figure D-1 Sensitivity of cumulative tile flow, Q_{tc}, cumulative soil to groundwater percolation rate, G_c, and mean soil saturated

1267   storage elevation, SS, to capillary fringe thickness, T_{CF} (a) capillary fringe drainable water, φ_c (b), soil hydraulic conductivity,

1268 K (c), soil thickness, T_{SL} (d), sine function amplitude, A (e) and sine function intercept, B (f).

1269

1270   *D.1.1 Sensitivity to capillary fringe thickness*

1271   To gauge sensitivity to capillary fringe thickness T_{CF}, flow rates and the SS were analyzed for T_{CF}

1272   ranging 0 to 1600 mm. Figure D-1a indicates that as T_{CF} increases, both cumulative tile flow (Q_{tc})

1273   and mean soil saturated storage (SS) decline. The SS drop is sharper for T_{CF} beyond 900 mm.

1274   Beyond this thickness, Q_{tc} stabilizes at a minimal value. A negative SS indicates its position below

1275   the tile pipe. G_c remains consistent despite T_{CF} variations.

1276

1277   *D.1.2 Sensitivity to capillary fringe drainable water*

1278   With rising φ_c both Q_{tc} and SS surge (Figure D-1b). As φ_c ascends from 0.005 to 0.45, Q_{tc} jumps

1279   from 1300 mm to 1900 mm and SS from -0.45 m to -0.25 m (Figure D-1b). G_c stays constant,

1280   irrespective of φ_c fluctuations.

1281

1282   *D.1.3 Sensitivity to soil hydraulic conductivity*

65

1283   Increasing soil hydraulic conductivity (K) from 0 to 10 mm hr^{-1}leads to a surge in Q_{tc} and a drop

1284   in SS (Figure D-1c). However, adjusting K from 10 to 50 mm hr^{-1} results in leveling off slopes for

1285 Q_{tc} and SS, especially when $K>$ 20mm hr^{-1}. Both metrics are acutely responsive to K when K is

1286   below 10 mm hr^{-1} but become non-responsive beyond 20mm hr^{-1}. G_c's response to K remains

1287   neutral.

1288

1289   *D.1.4 Sensitivity to soil thickness*

1290   Similar to K, a rise in T_{SL} from 1500mm to 15000 mm cause Q_{tc} to rise and SS to decline (Figure

1291   D-1d). The most significant rate of change for both metrics occurs between 1500 to 5000 mm T_{SL}.

1292   Beyond 5000 mm, changes flatten. G_c shows no response to T_{SL}variations.

1293

1294   *D.1.5 Sensitivity to sine function amplitude*

1295   Increasing the sine function amplitude, A, from -0.03 to 0 mm hr^{-1} pushes both Q_{tc} and SS increase

1296   and reach to their maximum at A=0 (Figure D-1e). But as A rises from 0 to 0.06 mm hr^{-1}, they both

1297   decline. In contrast, G_c descends to its lowest (400 mm) when A shifts from -0.03 to 0 and then

1298   increases to 900 mm as A hits 0.063.

1299

1300   *D.1.6 Sensitivity to sine function intercept*

1301   Both Q_{tc} and SS ascend with the growth in sine function's intercept, B. Increasing B from -0.015

1302   to 0.005 mm hr^{-1}sees G_c descend. During this B increase, Q_{tc} expands from 1100 to 2400 mm,

1303   while G_c shrinks from 1400 to 0 mm. It seems the sum of Q_{tc} and G_c might be constant. This

1304   suggests that water either drains through the tile pipe or percolates through the soil bottom.

1305 Q_{tc}, and SS appear sensitive to all six module parameters, but G_c only to A and B.

1306

D.2 Module parameter evaluation for new sites

1307

1308   As discussed in section 2.5, initial values for K, T_{CF} and φ_c can be determined by soil grain-size

1309   distribution. Parameters less explored in past research for new sites include the sine function's

1310   amplitude (A), intercept (B), and time delay (D_d).

1311

1312   *D.2.1 Evaluating sine function's A and B*

1313   If no percolation exists from the soil's bottom to groundwater and $G_{y,i}$ is zero, both A and B should

1314   be zero. However, if percolation or interactions between soil and groundwater occurs, A and B

1315   need calibration assessment. Before this, reasonable initial values and bounds must be set.

1316   From this study's findings, A and B should fall between the mean hourly difference of infiltration

1317   and observed tile flow rates. For instance, observed hourly rates for infiltration and tile flow at our

1318   site are 0.07 and 0.03 mm hr^{-1}. Thus, A's and B's initial values should range from -0.04 to 0.04

1319   mm hr^{-1}. Negative A and B values indicate outflow from soil to groundwater and vice versa. Initial

1320   values were set at 10% of the range limits: -0.004 for B and 0.004 for A. Eventually, B and A were

1321   adjusted to -0.005 and 0.025 mm hr^{-1}.

1322

1323   *D.2.2 Assessment of sine function's time delay*

1324   The sine function begins on the first Julian day. If its peak occurs around 91st Julian day (three

1325   months later), its minimum should be on the 274th day. If the peak comes later, say the 111th day,

1326   a 20-day delay is present. This delay should mirror in both function's minima and maxima. In this

1327   case the minimum would be on day 294. This delay aligns with the soil water table's peak annual

1328   fluctuations. When no observed fluctuations exist, the delay can be calibrated. A sensible initial

1329   delay can be ascertained by examining the study site's water table elevations, fitting a sine

1330   function, and noting the peak's Julian day annually.